Work Order No. 582-23-42440-034
Contract No. 582-19-90500
Tracking No. 2023-03
Task 7.2

Prepared for:

Texas Commission on Environmental Quality
12100 Park 35 Circle MC 164
Austin, TX 78753

Prepared by:

Ramboll US Consulting, Inc.
7250 Redwood Blvd., Suite 105
Novato, California 94945

June 23, 2023

Fire Emission Inventory (FEI) Processing

Final Report

PREPARED UNDER A CONTRACT FROM THE
TEXAS COMMISSION ON ENVIRONMENTAL QUALITY

The preparation of this document was financed through a contract from the State of Texas through the Texas Commission on Environmental Quality.
The content, findings, opinions and conclusions are the work of the author(s) and do not necessarily represent findings, opinions or conclusions of the TCEQ.

RAMBOLL

Fire Emission Inventory (FEI) Processing

Final Report

Ramboll
7250 Redwood Boulevard
Suite 105
Novato, CA 94945
USA

T +1 415 899 0700
https://ramboll.com

Contents

Appendix

Table of Figures

Table of Tables

LIST OF ARONYMS AND ABBREVIATIONS

3-D	Three-dimensional
ABI	Advanced Baseline Imager
ACM2	Asymmetric Convective Mixing, version 2
AFS	Aerometric information retrieval system Facility Subsystem
AIRS	Aerometric Information Retrieval System
AM	Ante-meridian
AOD	Aerosol Optical Depth
AQ	Air Quality
AQRP	Air Quality Research Program
BC	Black Carbon
CA	California
CAM-Chem	Community Atmosphere Model with Chemistry
CAMx	Comprehensive Air quality Model with extensions
CAMS	Copernicus Atmospheric Monitoring Service
CAMS	Continuous Ambient Monitoring Stations
CB6r4	Carbon Bond version 6, Revision 4
CB6r5	Carbon Bond version 6, Revision 5
CB7r1	Carbon Bond version 7, Revision 1
CDT	Central Daylight Time
CF2	Coarse/Fine 2-mode particulate matter chemistry
C-IFS	Composition Integrated Forecasting System
cm	centimeter
CMAQ	Community Multiscale Air Quality Model
CO	Carbon Monoxide
CONUS	CONtinental US
CST	Central Standard Time
CSV	Comma Separated Value file
EBI	Euler Backward Iterative solver
ECMWF	European Centre for Medium-Range Forecasts
EPA	Environmental Protection Agency
EPS3	Emissions Processing System, version 3
FDDA	Four Dimensional Data Assimilation
FEER	Fire Energetics and Emissions Research
FEI	Fire Emission Inventory
FINN	Fire INventory from NCAR
FRP	Fire Radiative Power
g	gram
GEOS	Goddard Earth Observing System
GEOS-Chem	Goddard Earth Observing System Chemical global model
GFAS	Global Fire Assimilation System
GIS	Geographic Information System
GOES	Geostationary Operational Environmental Satellite
HGB	Houston-Galveston-Brazoria
HRRR-Smoke	High Resolution Rapid Refresh model with smoke
IS4FIRES	Integrated monitoring and modelling System for wildland FIRES project
Ix	Inorganic iodine
JPSS	Joint Polar Satellite System
kg	kilogram

km	kilometer
m	meter
MDA8	Maximum Daily Average 8-hour
MERRA	Modern-Era Retrospective analysis for Research and Applications
MISR	Multi-angle Imaging SpectroRadiometer
MODIS	MODerate resolution Imaging SpectroRadiometer
mol	mole
MPE	Model Performance Evaluation
NASA	National Aeronautics and Space Administration
NCAR	National Center for Atmospheric Research
netCDF	network Common Data Format
NAAQS	National Ambient Air Quality Standard
NMB	Normalized mean bias
NME	Normalized mean error (unsigned, or gross)
NOx	Nitrogen oxides
NRT	Near-Real Time
NRTEEM	Near-Real Time Exceptional Event Model
OC	Organic Carbon
OM	Organic Mass
PBL	Planetary Boundary Layer
PBL500	Planetary Boundary Layer height plus 500 meters
PDT	Pacific Daylight Time
PiG	Plume-in-Grid
PM	Post-meridian
PM	Particulate Matter
$PM_{2.5}$	Particulate Matter less than 2.5 microns
ppb	parts per billion
PPM	Piecewise Parabolic Method
QFED	Quick Fire Emissions Dataset
RAVE	Regional Advanced baseline imager and Visible infrared imaging radiometer suite fire Emissions
s	second
SIP	State Implementation Plan
SMOKE	Sparse Matrix Operator Kernel Emissions
SST	Sea Surface Temperature
TCEQ	Texas Commission on Environmental Quality
ug	microgram
US	United States
VIIRS	Visible Infrared Imaging Radiometer Suite
VOC	Volatile organic compounds
W	Watt
WACCM	Whole Atmosphere Community Climate Model
Westar	Western States Air Resources Council
WRAP	Western Regional Air Partnership
WRF	Weather Research and Forecasting model
WRF-Chem	Weather Research and Forecasting model with Chemistry

EXECUTIVE SUMMARY

Fires are large emission sources affecting ozone and particulate matter concentrations over regional scales, and therefore accurate Fire Emission Inventories (FEIs) are needed for exceptional event analyses and State Implementation Plan (SIP) modeling. Emission estimates from currently available FEIs can differ by an order of magnitude so the decision of which FEI to include in modeling may have a significant impact on modeled air quality. The TCEQ has relied upon the Fire INventory from NCAR (FINN) to characterize fire emissions in recent modeling efforts. In a previous project with the TCEQ, Ramboll (2022b) developed a Python-based tool to process three different global FEIs into model-ready inputs, which allows the TCEQ to choose among other FEIs to improve model performance. The original version of the tool could process: 1) FINN2.5; 2) Global Fire Assimilation System version 1.2 (GFAS1.2); and 3) Quick Fire Emissions Dataset version 2.5 (QFED2.5). Under this project, we developed the capability to process a fourth FEI, Fire Energetics and Emissions Research (FEER1.0), and implemented additional options for temporal emission allocation and vertical plume rise schemes. This project also evaluated photochemical model performance using the different FEIs from which to make recommendations on the FEI(s) to include in SIP modeling.

As requested by TCEQ, we applied TCEQ's modeling platform for April-May 2019, replacing only the fire emissions generated by the recently updated Python FEI processor. TCEQ's modeling using the Comprehensive Air quality Model with extensions (CAMx; Ramboll, 2022c) showed large positive ozone biases related to FINN fire emissions throughout April and May of 2019 when transport of smoke from biomass burning in Mexico and Central America was frequent.

Our testing confirmed that FINN2.5 resulted in similarly large positive ozone biases. However, the three Fire Radiative Power (FRP)-based FEIs (GFAS, QFED, FEER) all showed substantially smaller ozone biases and overall better statistical agreement with observations. We identified GFAS1.2 as the best representation of fires due to overall ozone model performance and its reporting of useful parameters such as FRP and vertical plume information. We then conducted additional testing using fire emission inputs based on all four combinations of vertical and temporal allocation schemes applied to the GFAS1.2 FEI. Ozone and fine particulate matter ($PM_{2.5}$) concentrations were nearly identical across the four tests given long range transport that moderates effects from plume rise and temporal treatments. Therefore, we cannot make recommendations from these tests regarding optimal processor configuration options.

Finally, Ramboll evaluated potential methods, benefits and challenges involved in developing a consensus FEI. After a literature review and consideration of the limitations of the FEIs, as well as our limited modeling application, we cannot recommend a particular strategy for developing a consensus FEI. We therefore recommend GFAS1.2 as an alternative to a consensus approach. This recommendation is based on the two-month period evaluated in this study and could change pending additional modeling for different years, seasons, or regions. For future work, we recommend modeling different seasons and years and including additional FEIs as they become available.

Additionally under this project, three remote technical workshops were developed and delivered to TCEQ staff on best practices for meteorological and photochemical modeling and evaluation.

1.0 INTRODUCTION

1.1 Background

Fires are large emission sources affecting ozone and particulate matter concentrations over regional scales, and therefore accurate Fire Emission Inventories (FEIs) are needed for exceptional event analyses and State Implementation Plan (SIP) modeling. Emissions estimates from currently available FEIs can differ by an order of magnitude so the decision of which FEI to include in modeling may have a significant impact on modeled air quality. The TCEQ has relied upon the Fire INventory from NCAR (FINN[1]) to characterize fire emissions in recent modeling efforts. In a previous project with the TCEQ, Ramboll (2022b) developed a Python-based tool to process three different global FEIs into model-ready inputs, which allows the TCEQ to choose among other FEIs to improve model performance. The original version of the tool could process: 1) FINN2.5; 2) Global Fire Assimilation System version 1.2 (GFAS1.2[2]); and 3) Quick Fire Emissions Dataset version 2.5 (QFED2.5[3]). Under this project, we developed the capability to process a fourth FEI, Fire Energetics and Emissions Research (FEER1.0[4]) and implemented additional options for temporal emission allocation and vertical plume rise schemes. This project also evaluated photochemical model performance using the different FEIs from which to make recommendations on the FEI(s) to include in SIP modeling.

1.2 Project Objectives

The purpose of this project was to further develop the FEI processor to support air quality modeling and to evaluate FEI impacts on photochemical model performance. This project helped inform decisions on which emissions inventories are best suited for modeling platform development.

[1] https://www2.acom.ucar.edu/modeling/finn-fire-inventory-ncar

[2] https://www.ecmwf.int/en/forecasts/dataset/global-fire-assimilation-system

[3] https://gmao.gsfc.nasa.gov/research/science_snapshots/global_fire_emissions.php

[4] https://feer.gsfc.nasa.gov

2.0 FEI PROCESSOR UPDATES

2.1 FEI Summary

The FEI processor was originally developed in 2022 and was designed to generate fire emissions for the following three global FEI products:

- Fire Inventory from NCAR version 2.5 (FINN2.5)
- Global Fire Assimilation version 1.2 (GFAS1.2)
- Quick Fire Emissions Dataset version 2.4 (QFED2.5)

For this project, we added the capability to process one additional FEI product:

- Fire Energetics and Emissions Research version 1.0 (FEER1.0)

Table 2-1 summarizes key characteristics of these four FEIs. We also summarize a new FEI, Regional ABI and VIIRS fire Emissions version 1.0 (RAVE1.0), which we have utilized as a resource to develop landcover-specific temporal allocation factors and fire radiative power (FRP) estimates from CO emissions. We do not include RAVE1.0 in the FEI processor because it does not have emissions prior to 2021, and it therefore cannot be used to support TCEQ's 2019 SIP modeling. However, RAVE has useful supporting datasets to support the processor upgrades.

Table 2-1. Summary of key characteristics of FEIs.

FEI	Horizontal Resolution	Timeframe	Frequency	Approach	Burned Area/FRP Methodology	Emissions Species	Modeling Applications
FINN2.5	1 km^2 (text product) and 0.1°×0.1° (gridded product)	2002–2021	Daily through 2020; previous calendar year available each July	Burned area	Estimated by active MODIS and VIIRS fire counts: 0.75 km^2 for savanna at each fire pixel, 1 km^2 for other types	NOx, VOC, CO, SO2, NH3, OC, $PM_{2.5}$	FINN1.0: TCEQ NRTEEM (2017-2020); WACCM real time forecasts FINN2.2: TCEQ 2019 SIP modeling platform
GFAS1.2	0.1°×0.1°	2003–present	Daily with 24-hour lag	FRP	MODIS	NOx, VOC, CO, SO2, NH3, OC, BC, $PM_{2.5}$	CAMS C-IFS
QFED2.5	0.1°×0.1°	2000–Present	Daily with 1-month lag	FRP	MODIS	NOx, VOC, CO, SO2, OC, BC, $PM_{2.5}$	GEOS-Chem; CAM-chem
FEER1.0	0.1°×0.1°	2003–Present	Daily with 1-month lag	FRP	From GFASv1.2 (Kaiser et al., 2012)	NOx, VOC, CO, SO2, NH3, OC, BC, $PM_{2.5}$	Fire research; climate impacts; Northern Sub-Saharan research
RAVE1.0	3 km^2 over North America	2021–Present	Hourly with 24-hour lag	FRP	GOES, VIIRS	NOx, total VOC, CO, SO2, NH3, OC, BC, $PM_{2.5}$	HRRR-Smoke; CMAQ; WRF-Chem

2.1.1 FINN2.5

The TCEQ uses FINN2.2 to characterize and estimate fire emissions for their 2019 SIP modeling platform. As of this writing (June 2023), FINN2.5 (released February 2022) is available through 2021. FINN2.5's satellite pixel-based text product has 1 km^2 horizontal resolution, the highest of any of the FEIs compatible with the FEI processor. Ramboll used FINN1.0 for TCEQ Near Real-Time modeling (NRT; Johnson et al., 2013, 2015, 2016) and TCEQ Near Real-Time Exceptional Event Modeling (NRTEEM; Johnson et al., 2017, 2018, 2019; Ramboll, 2020). NCAR currently uses FINN1.0 for Whole Atmosphere Community Climate Model (WACCM) real time global forecasts[5].

Modeling projects originally performed in the Western U.S. by the Western Regional Air Partnership/Western States Air Resources Council (WRAP/WESTAR), and later adopted in TCEQ's SIP modeling, processed FINN fire emissions as point sources through Fortran-based preprocessors. These processors create Aerometric Information Retrieval System (AIRS) Facility Subsystem (AFS) files used as inputs to the Emissions Processing System, version 3 (EPS3). EPS3 modules were designed to process FINN fires using temporal and vertical allocation schemes developed by WRAP/WESTAR. Previously, the FINN2.5 emissions product was only available as a CSV text file, where fire emissions are represented as points corresponding to the centers of MODIS and/or VIIRS satellite burn scar pixels. However, NCAR recently started distributing FINN2.5 emissions as a global 0.1° gridded netCDF product[6], which we utilize instead of the point-based emissions in this updated distribution. The format and structure of this new FINN2.5 product are consistent with the GFAS1.2, QFED2.5 and FEER1.0 products.

2.1.2 GFAS1.2

GFAS multiplies FRP from MODIS Aqua/Terra satellite measurements by land cover specific conversion factors to obtain dry matter combustion rate estimates. GFAS then employs a sophisticated filtering system that masks spurious FRP signals from volcanoes, gas flaring and other industrial activity. GFAS includes vertical parameters – plume bottom, plume top and mean altitude of maximum injection height (described in Remy et al., 2017), all of which are derived from a plume rise model. GFAS also provides a separate injection height from IS4FIRES (Remy et al., 2017). As with the fire emissions, these vertical parameters have daily resolution which correspond to early afternoon. The European Centre for Medium-Range Forecasts (ECMWF) Composition Integrated Forecasting System (C-IFS) of Copernicus Atmospheric Monitoring Service (CAMS) utilizes GFAS1.2 for global real time fire and smoke forecasts. GFAS1.2 is available in near real-time at 0.1° resolution.

2.1.3 QFED2.5

Similar to GFAS, QFED uses FRP measurements from MODIS Aqua/Terra satellites. QFED calculates emissions using scaling factors applied to the FRP measurements. These scaling factors are developed from comparisons of aerosol optical depth (AOD) between NASA's Goddard Earth Observing System (GEOS) model and MODIS measurements across different regions (Darmenov and da Silva, 2015). QFED2.5 applies a sophisticated treatment of cloud obscured land areas and is used in NASA's NRT GEOS model and Modern-Era Retrospective analysis for Research and Applications version 2 (MERRA-2) reanalyses (Randles et al., 2017). NCAR's Community Atmosphere Model with chemistry (CAM-chem) also utilizes QFED, and QFED is an optional FEI for GEOS-Chem. QFED2.5 emissions are available daily for the entire previous calendar month and have 0.1° resolution.

[5] https://www2.acom.ucar.edu/modeling/finn-fire-inventory-ncar

[6] https://www.acom.ucar.edu/Data/fire/

2.1.4 FEER1.0

FEER1.0 uses GFAS1.2 FRP data and multiplies by emission coefficients to obtain smoke aerosol emissions (Ichoku and Ellison, 2014). These emission coefficients were formulated from a detailed analysis of MODIS AOD and winds from NASA's MERRA reanalysis dataset (Rienecker et al., 2011). Scaling factors for chemical species including OC, BC, NOx, VOC, SO2 and CO are then applied to the smoke aerosol emissions to obtain emissions for these species. Fire research, climate impacts and Northern Sub-Saharan research all utilize FEER emissions. As with QFED2.5, FEER1.0 daily emissions are available for the entire previous calendar month and have 0.1° resolution.

2.1.5 RAVE1.0

RAVE1.0 is a new FEI product (available 2021 onward) that utilizes a new algorithm to generate hourly 0.03° fire emissions by fusing temporally resolved GOES Advanced Baseline Imager (ABI) FRP and fine spatial-resolution (375 m) FRP from the Visible Infrared Imaging Radiometer Suite (VIIRS) on the Joint Polar Satellite System (JPSS) satellites (Li et al., 2022). RAVE1.0 is available as a near real-time product that covers North America and a "re-processed" historical product that covers the continental U.S. only. Hourly emissions are produced from land cover and ecoregion-specific FRP diurnal cycles using 5-minute GOES ABI FRP measurements. RAVE's combination of high temporal and spatial resolution is unique and thus appears well-suited for high resolution photochemical modeling. However, since RAVE1.0 does not have emissions prior to 2021, it cannot be used for this project to support TCEQ's 2019 SIP modeling. We instead use the high resolution landcover and landcover-specific diurnal profiles developed by the RAVE team in this project.

2.2 FEI Tool Processing Steps

This section describes each of the FEI processing steps (regridding, chemical species mapping, temporal allocation and vertical plume rise) in detail, as shown in the blue hatched box in Figure 2-1. Specific instructions for how to run the Python tool and execute necessary preprocessing steps are provided in the User Guide. The FEI processor provides output gridded emissions in CAMx-ready 3-D netCDF format.

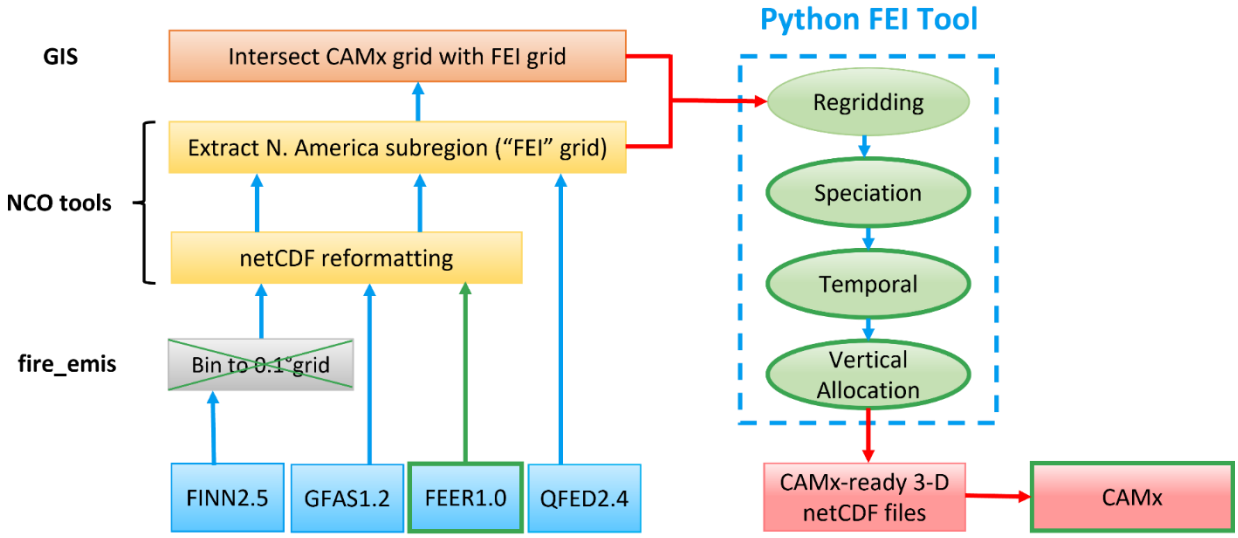

Figure 2-1. Flow diagram for processing global gridded FEIs. Updates for the 2023 project shown in green.

2.2.1 Regridding

The regridding step maps fire emissions from the 0.1° resolution "FEI grid" (spans +7.9° to +65° latitude and -150° to -40° longitude) to a target CAMx modeling grid using a cross-reference grid mapping file produced by a Geographic Information System (GIS) intersection. The grid mapping file contains areas for each FEI grid cell that intersects each target CAMx grid cell. We provide instructions for performing this GIS intersection step in the User Guide. Because each FEI product contains emissions expressed as fluxes (emissions in kg m^{-2} s^{-1} or molecules cm^{-2} s^{-1}), the regridding algorithm simply multiplies each flux by the associated mapped fractional FEI grid cell area and sums over all FEI areas to obtain emission rate totals (kg s^{-1} or moles s^{-1}) across each CAMx grid cell. Because the FEI emission fluxes are distributed in 0.1° grid cells, emission fluxes for small fires (smaller than ~100 km^2) fires can be overestimated. Because the FEI extent is common to the four FEIs used in this project, only one cross-reference file needs to be produced for each target CAMx domain. The output from this step creates gridded fire emissions for the target CAMx domain.

For this project, we developed the capability to re-grid North America landcover from the RAVE FEI product[7] to each modeling grid – see Continental US (CONUS) map in Figure 2-2. The RAVE team aggregated the 2019 MODIS 500 m landcover product to RAVE's 0.03° resolution over North America. The landcover fields are time invariant and therefore only need to be regridded once for each modeling domain. We provide these landcover fields for each domain along with the code distribution. These fields are used in the new RAVE landcover temporal allocation scheme discussed later in this chapter.

[7] https://sites.google.com/view/rave-emission/ancillary-data

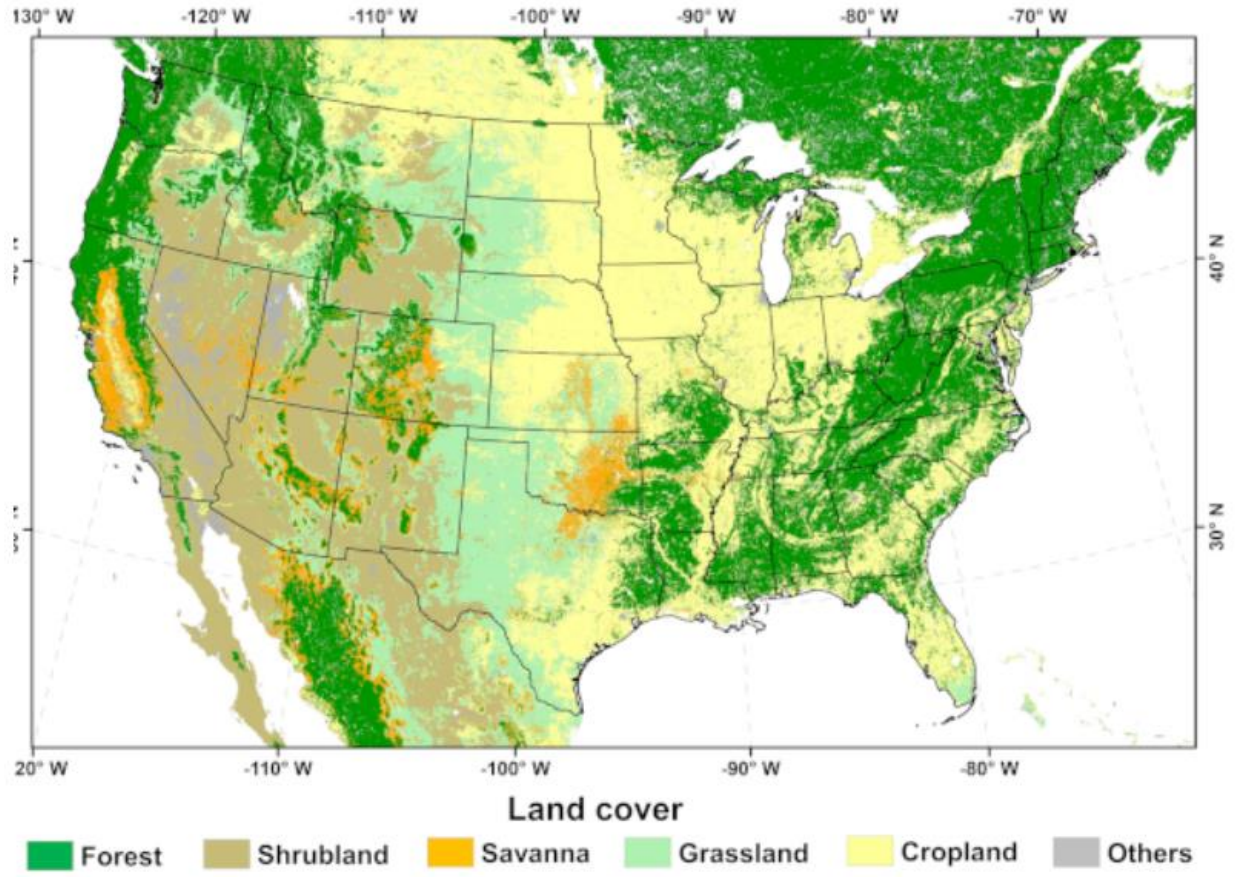

Figure 2-2. Map of landcover used by the RAVE FEI and mapped to TCEQ CAMx modeling domains for this project.

2.2.2 Chemical Species Mapping

After the regridding step, the FEI processor maps the available chemical species in the fire emissions file to the desired CAMx mechanism species. Table 2-2 lists the chemical species mapping from FINN2.5 to the CAMx Carbon Bond version 6, Revision 4 (CB6r4) chemical mechanism. We provide similar mapping tables for GFAS1.2 in Table 2-3, QFED2.5 in Table 2-4 and FEER1.0 in Table 2-5. We provide these chemical species mappings as an input CSV file to the tool, which can be updated as needed. The MW column represents the molecular weight of the FEI species to convert from mass to moles and a scale column that converts between the FEI species and CAMx species. All GFAS1.2 and QFED2.5 and FEER1.0 species (aerosols and gases) use emissions fluxes expressed in mass units, so molecular weights are applied to gases to convert from mass to moles for these three FEIs. FINN2.5 uses molecules as units for aerosols and gases – therefore, we set the MW column to 1 for gases, and apply a molecular weight of 12 g mol^{-1} for aerosols (see Table 2-2), consistent with guidance on NCAR's FINN website[8].

The species mapping in each of the three tables account for a more realistic (rapid) NOx to NOy conversion in smoke plumes, an approach obtained from the 2015 Texas Air Quality Research Program

[8] https://www2.acom.ucar.edu/modeling/finn-fire-inventory-ncar

(AQRP) Fires project (McDonald-Buller et al., 2015). Additionally, all mappings assume an organic mass to organic carbon (OM/OC) ratio of 1, due to lack of clarifying information.

The CSV file also contains a comments column which we use to document any assumptions made about the FEI species. The FEI tool distribution contains mappings for the FINN1.0 product (available in near-real time) as well as a separate CSV file containing mappings for all four FEIs to the CAMx Carbon Bond version 7, Revision 1 (CB7r1; Ramboll, 2022a) chemical mechanism. This processing step also converts the emission rate from s^{-1} to day^{-1}, so that output from this step contains daily fire emissions for the target grid for all CAMx species.

Table 2-2. Chemical species mapping from FINN2.5 to CAMx CB6r4 chemical mechanism.

CAMx Species	FINN2.5 Species	Scale	MW (g/mol)	G(as) or A(erosol)	Comment
AACD	CH3COOH	1	1	G	# acetic acid
ACET	CH3COCH3	1	1	G	
ALD2	CH3CHO	1	1	G	
BENZ	BENZENE	1	1	G	# FINN2.5 maps toluene xylene and benzene explicitly
CH3CN	CH3CN	1	1	G	#not a CAMx model species but retained as potential tracer
CO	CO	1	1	G	
CRES	CRESOL	1	1	G	
CRES	XYLOL	1	1	G	# dimethyl phenol from xylenes oxidation
CRES	PHENOL	1	1	G	
ECH4	CH4	1	1	G	
ETH	C2H4	1	1	G	
ETHA	C2H6	1	1	G	
ETHY	C2H2	1	1	G	
ETOH	C2H5OH	1	1	G	
FACD	HCOOH	1	1	G	
FORM	CH2O	1	1	G	
GLYD	GLYALD	1	1	G	
HCN	HCN	1	1	G	#not a CAMx model species but retained as potential tracer
HNO3	NO	0.18	1	G	#mapping developed for AQRP FINN2.0 beta project
HNO3	NO2	0.18	1	G	#mapping developed for AQRP FINN2.0 beta project
HONO	HONO	1	1	G	# added in FINN2.5
IOLE	BIGENE	0.5	1	G	# lumped alkenes C>3; used mapping from WACCM (0.5 IOLE 0.5 OLE 0.5 PAR)
ISOP	ISOP	1	1	G	
ISPD	MACR	1	1	G	
ISPD	MVK	1	1	G	
KET	HYAC	1	1	G	#hydroxyacetone C3H6O2
KET	MEK	1	1	G	
MEOH	CH3OH	1	1	G	
MGLY	CH3COCHO	1	1	G	
NH3	NH3	1	1	G	
NO	NO	0	1	G	#mapping developed for AQRP FINN2.0 beta project
NO	NO2	0	1	G	#mapping developed for AQRP FINN2.0 beta project
NO2	NO	0.736	1	G	#mapping developed for AQRP FINN2.0 beta project
NO2	NO2	0.736	1	G	#mapping developed for AQRP FINN2.0 beta project
NTR2	NO	0.02	1	G	#mapping developed for AQRP FINN2.0 beta project

CAMx Species	FINN2.5 Species	Scale	MW (g/mol)	G(as) or A(erosol)	Comment
NTR2	NO2	0.02	1	G	#mapping developed for AQRP FINN2.0 beta project
OLE	BIGENE	0.5	1	G	# lumped alkenes C>3; used mapping from WACCM (0.5 IOLE 0.5 OLE 0.5 PAR)
OLE	C3H6	1	1	G	
OPEN	BZALD	1	1	G	# benzaldehyde
PANX	NO	0.008	1	G	#mapping developed for AQRP FINN2.0 beta project
PANX	NO2	0.008	1	G	#mapping developed for AQRP FINN2.0 beta project
PAR	BIGALK	5	1	G	#lumped alkanes C>3
PAR	BIGENE	0.5	1	G	# lumped alkenes C>3; used mapping from WACCM (0.5 IOLE 0.5 OLE 0.5 PAR)
PAR	C3H6	1	1	G	
PAR	HYAC	2	1	G	#hydroxyacetone C3H6O2
PAR	MEK	3	1	G	
PAR	PHENOL	-1	1	G	
PAR	XYLOL	1	1	G	# dimethyl phenol from xylenes oxidation
PRPA	C3H8	1	1	G	
SO2	SO2	1	1	G	
TERP	APIN	1	1	G	
TERP	BPIN	1	1	G	
TERP	LIMON	1	1	G	
TERP	MYRC	1	1	G	# myrcene
TOL	TOLUENE	1	1	G	# FINN2.5 maps toluene xylene and benzene explicitly
XYL	XYLENES	1	1	G	# FINN2.5 maps toluene xylene and benzene explicitly
CPRM	PM10	1	12	A	
CPRM	PM25	-1	12	A	
FPRM	BC	-1	12	A	
FPRM	OC	-1	12	A	
FPRM	PM25	1	12	A	
PEC	BC	1	12	A	
POA	OC	1	12	A	

Table 2-3. Chemical species mapping from GFAS1.2 to CAMx CB6r4 chemical mechanism.

CAMx Species	GFAS1.2 species	Scale	MW (g/mol)	G(as) or A(erosol)	Comment
ACET	c3h6ofire	1	58.09	G	
ALD2	c2h4ofire	1	44.06	G	
BENZ	c6h6fire	1	78.12	G	
CO	cofire	1	28.01	G	
DMS	c2h6sfire	1	62.13	G	
ECH4	ch4fire	1	16.05	G	
ETH	c2h4fire	1	28.05	G	
ETHA	c2h6fire	1	30.08	G	
ETOH	c2h5ohfire	1	46.08	G	
FORM	ch2ofire	1	30.03	G	
HNO3	noxfire	0.18	46	G	#mapping developed for AQRP FINN2.0 beta project
IOLE	c4h8fire	0.5	56.11	G	#assume 50/50 split between OLE/IOLE with PAR updated to reflect difference in carbon number
IOLE	c5h10fire	0.5	70.13	G	#assume 50/50 split between OLE/IOLE with PAR updated to reflect difference in carbon number
IOLE	c6h12fire	0.5	84.16	G	#assume 50/50 split between OLE/IOLE with PAR updated to reflect difference in carbon number
IOLE	c8h16fire	0.5	112.21	G	#assume 50/50 split between OLE/IOLE with PAR updated to reflect difference in carbon number
ISOP	c5h8fire	1	68.13	G	
MEOH	ch3ohfire	1	32.05	G	
NH3	nh3fire	1	17.04	G	
NO	noxfire	0	46	G	#mapping developed for AQRP FINN2.0 beta project
NO2	noxfire	0.736	46	G	#mapping developed for AQRP FINN2.0 beta project
NTR2	noxfire	0.02	46	G	#mapping developed for AQRP FINN2.0 beta project
OLE	c3h6fire	1	42.09	G	
OLE	c4h8fire	0.5	56.11	G	#assume 50/50 split between OLE/IOLE with PAR updated to reflect difference in carbon number
OLE	c5h10fire	0.5	70.13	G	#assume 50/50 split between OLE/IOLE with PAR updated to reflect difference in carbon number
OLE	c6h12fire	0.5	84.16	G	#assume 50/50 split between OLE/IOLE with PAR updated to reflect difference in carbon number
OLE	c8h16fire	0.5	112.21	G	#assume 50/50 split between OLE/IOLE with PAR updated to reflect difference in carbon number
PANX	noxfire	0.008	46	G	#mapping developed for AQRP FINN2.0 beta project
PAR	c3h6fire	1	42.09	G	
PAR	c4h8fire	1	56.11	G	#assume 50/50 split between OLE/IOLE with PAR updated to reflect difference in carbon number

CAMx Species	GFAS1.2 species	Scale	MW (g/mol)	G(as) or A(erosol)	Comment
PAR	c5h10fire	2	70.13	G	#assume 50/50 split between OLE/IOLE with PAR updated to reflect difference in carbon number
PAR	c6h12fire	3	84.16	G	#assume 50/50 split between OLE/IOLE with PAR updated to reflect difference in carbon number
PAR	c8h16fire	5	112.21	G	#assume 50/50 split between OLE/IOLE with PAR updated to reflect difference in carbon number
PAR	c4h10fire	4	58.12	G	
PAR	c5h12fire	5	72.15	G	
PAR	c6h14fire	6	86.18	G	
PAR	c7h16fire	7	100.2	G	
PRPA	c3h8fire	1	44.11	G	
SO2	so2fire	1	64.04	G	
TERP	terpenesfire	1	136.23	G	#assume MW 2*ISOP
TOL	c7h8fire	1	92.15	G	
XYL	c8h10fire	1	106.18	G	
CPRM	tpmfire	1	1	A	
CPRM	pm2p5fire	-1	1	A	
FPRM	pm2p5fire	1	1	A	
FPRM	bcfire	-1	1	A	
FPRM	ocfire	-1	1	A	#assume OC represents organic mass and not just organic carbon
PEC	bcfire	1	1	A	
POA	ocfire	1	1	A	#assume OC represents organic mass and not just organic carbon

Table 2-4. Chemical species mapping from QFED2.5 to CAMx CB6r4 chemical mechanism.

CAMx Species	QFED2.5 species	Scale	MW (g/mol)	G(as) or A(erosol)	Comment
ACET	ACET	1	58.09	G	
ALD2	ALD2	1	44.06	G	
PAR	ALK4	5	72.15	G	#assume petane for consistency with BIGALK in FINN
ETHA	C2H6	1	30.08	G	
PAR	C3H6	1	42.09	G	
OLE	C3H6	1	42.09	G	
PRPA	C3H8	1	44.11	G	
FORM	CH2O	1	30.03	G	
ECH4	CH4	1	16.05	G	
CO	CO	1	28.01	G	
PAR	MEK	3	72.11	G	
KET	MEK	1	72.11	G	
NH3	NH3	1	17.04	G	
NO	NO	0	30.01	G	#mapping developed for AQRP FINN2.0 beta project
NO2	NO	0.736	30.01	G	#mapping developed for AQRP FINN2.0 beta project
PANX	NO	0.008	30.01	G	#mapping developed for AQRP FINN2.0 beta project
NTR2	NO	0.02	30.01	G	#mapping developed for AQRP FINN2.0 beta project
HNO3	NO	0.18	30.01	G	#mapping developed for AQRP FINN2.0 beta project
SO2	SO2	1	64.04	G	
PEC	BC	1	1	A	
POA	OC	1	1	A	#assume OC represents organic mass and not just organic carbon
FPRM	PM25	1	1	A	
FPRM	BC	-1	1	A	
FPRM	OC	-1	1	A	#assume OC represents organic mass and not just organic carbon

Table 2-5. Chemical species mapping from FEER1.0 to CAMx CB6r4 chemical mechanism.

CAMx Species	QFED2.5 species	Scale	MW (g/mol)	G(as) or A(erosol)	Comment
ACET	Acet	1	58.09	G	
ALD2	MeCHO	1	44.06	G	
CO	CO	1	28.01	G	
ECH4	CH4	1	16.05	G	
ETHA	C2H6	1	30.07	G	
ETHY	C2H2	1	26.038	G	
FACD	CH2O2	1	46.025	G	
FORM	CH2O	1	30.026	G	
HCN	HCN	1	27.026	G	#not a CAMx model species but retained as potential tracer
HNO3	NOx	0.18	30.01	G	#mapping developed for AQRP FINN2.0 beta project; assume NO MW based on Table 1 in Andreae and Merlet
KET	MEK	1	72.11	G	
MEOH	CH4O	1	32.05	G	
NH3	NH3	1	17.04	G	
NO	NOx	0	30.01	G	#mapping developed for AQRP FINN2.0 beta project; assume NO MW based on Table 1 in Andreae and Merlet
NO2	NOx	0.736	30.01	G	#mapping developed for AQRP FINN2.0 beta project; assume NO MW based on Table 1 in Andreae and Merlet
NTR2	NOx	0.02	30.01	G	#mapping developed for AQRP FINN2.0 beta project; assume NO MW based on Table 1 in Andreae and Merlet
OLE	C3H6	1	42.09	G	
PANX	NOx	0.008	30.01	G	#mapping developed for AQRP FINN2.0 beta project; assume NO MW based on Table 1 in Andreae and Merlet
PAR	C3H6	1	42.09	G	
PAR	iBut	4	58.12	G	
PAR	MEK	3	72.11	G	
PAR	nBut	4	58.12	G	
PRPA	C3H8	1	44.097	G	
SO2	SO2	1	64.04	G	
CPRM	PM2.5	-1	1	A	#assume PM2.5 includes BC and OC
CPRM	TPM	1	1	A	#assume TPM includes all particulate matter
FPRM	BC	-1	1	A	
FPRM	OC	-1	1	A	#assume OC represents organic mass and not just organic carbon
FPRM	PM2.5	1	1	A	#assume PM2.5 includes BC and OC

2.2.3 Temporal Allocation

Next, the FEI processor distributes the daily total emissions to individual hours via a temporal profile. Figure 2-3 shows the single diurnal temporal profile provided with the initial distribution of the FEI processor. We developed this default profile to be used for all fire and fuel types. For this project, we developed a new option to utilize a set of landcover-specific diurnal temporal profiles from the RAVE FEI product[9] (see Figure 2-4). The RAVE team derived these profiles using GOES ABI FRP measurements aggregated to RAVE's 0.03° grid resolution over North America. We provide input files for both the default and RAVE landcover temporal profiles along with the code distribution.

[9] https://sites.google.com/view/rave-emission/diurnal-cycles

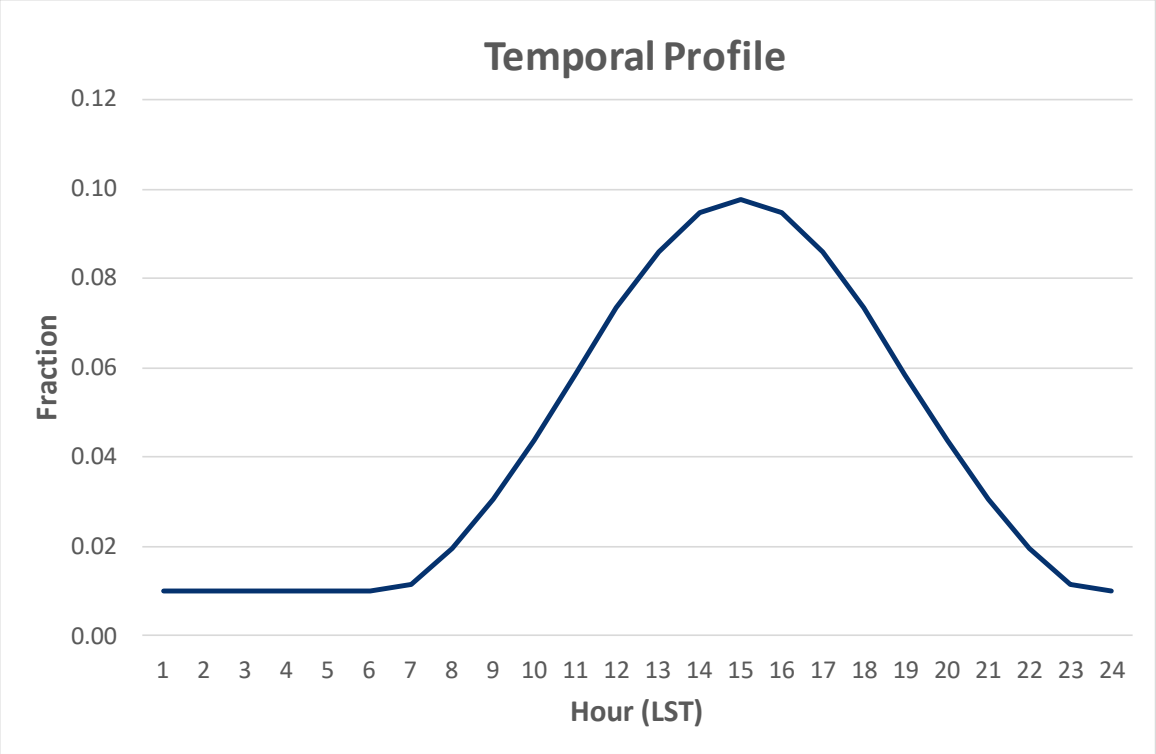

Figure 2-3. Default diurnal profile used to allocate fire emissions in the FEI processors.

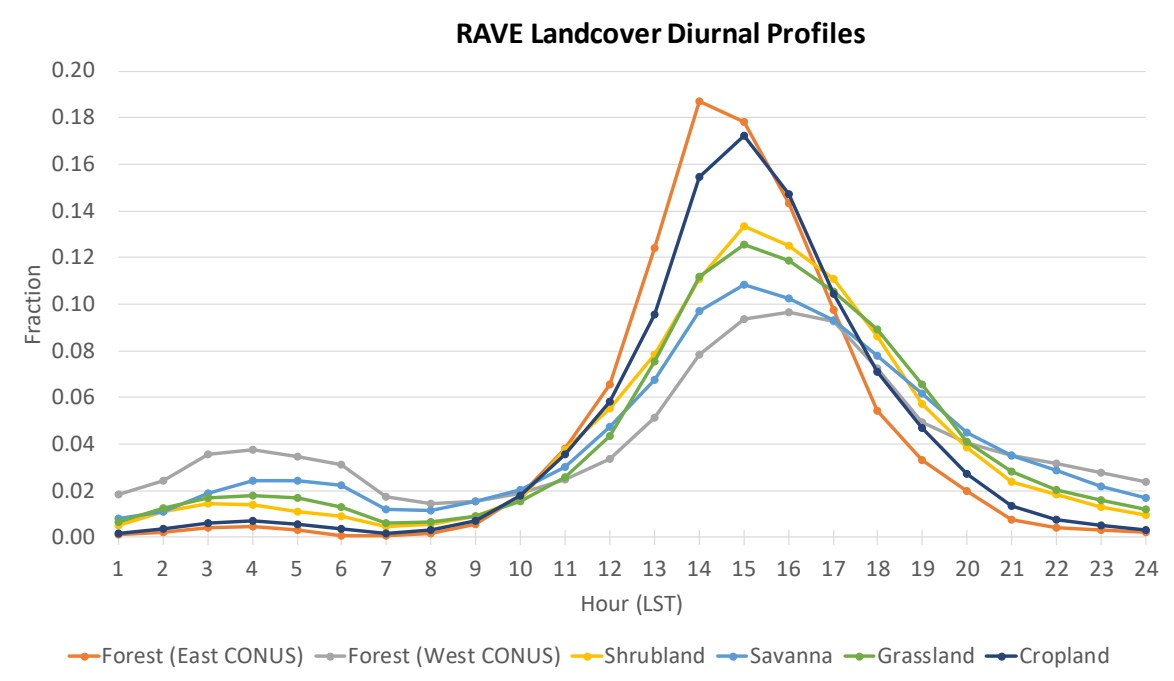

Figure 2-4. Landcover-specific diurnal profiles used in the RAVE FEI product[10] derived from GOES ABI FRP measurements.

[10] https://sites.google.com/view/rave-emission/diurnal-cycles

2.2.4 Vertical Allocation

The final step in the FEI processing allocates hourly fire emissions vertically. The initial release of the FEI processor included the PBL500 plume rise algorithm with adaptations to distribute emissions vertically between the ground surface and plume top. Wilkins et al. (2022) defines the PBL500 plume injection height as simply the PBL height plus 500 m.

The PBL500 plume rise algorithm (as well as another approach we refer to as Sofiev) predicts only the injection height or top of the smoke plume. We therefore developed a methodology similar to that used in the SMOKE-Briggs approach (Briggs, 1975), where we: 1) define the ground surface as the bottom of the smoke plume; 2) allocate 90% of the total column hourly emissions to the top 2/3 of the plume; and 3) allocate the remaining 10% of emissions to the bottom 1/3 of the plume. We distribute emissions in each CAMx model layer weighted by layer thickness. Figure 2-5 shows an example vertical profile for a grid cell with a PBL height of 2,000 m and 100 mol of total column CO emissions. The FEI processor uses this methodology for both the PBL500 and Sofiev vertical allocation schemes.

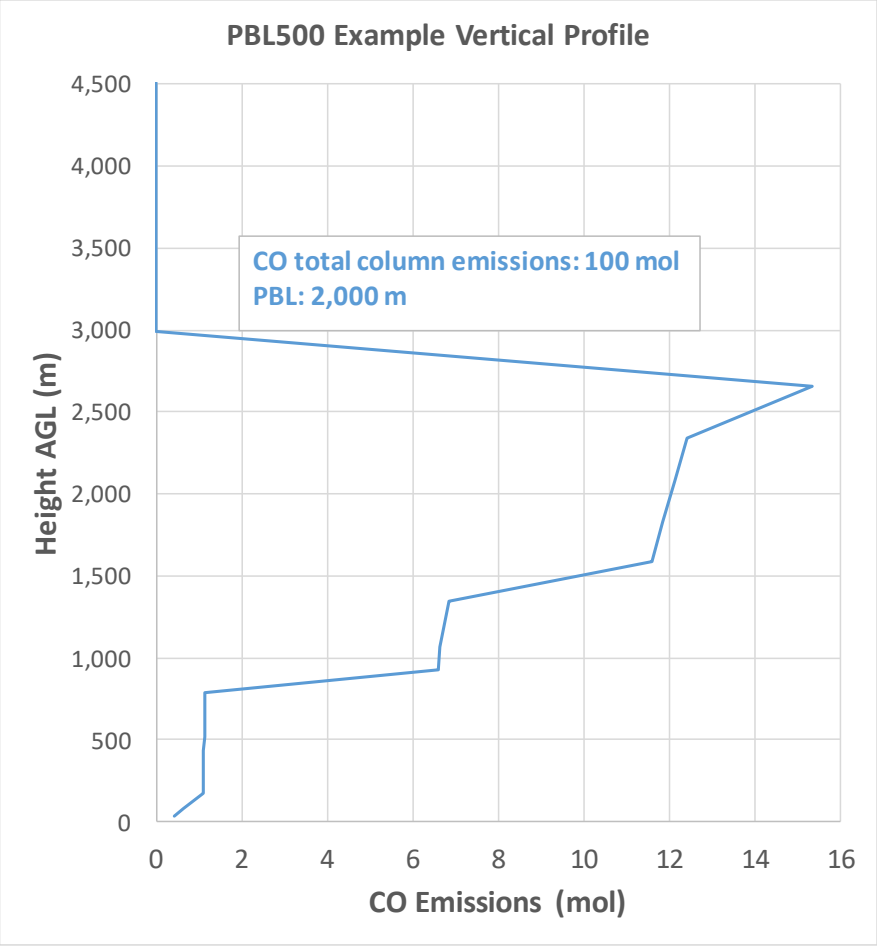

Figure 2-5. PBL500 example vertical profile showing vertical distribution of emissions where the total column CO emissions are 100 moles and PBL height is 2,000 m.

2.2.4.1 Sofiev Formulation

For this project, we implemented a modified version of the Sofiev plume rise algorithm as an alternative to the PBL500 scheme. Sofiev et al. (2012) derived an energy-balance parameterization of plume injection height that accounts for PBL mixing, power law dependence of fire intensity, and stability in the free troposphere. The Sofiev scheme includes 4 fitted tunable parameters to match observed plume heights by NASA's Multi-angle Imaging SpectroRadiometer (MISR). We provide the equation and definition of variables below:

$$H_P = \alpha H_{PBL} + \beta \left(\frac{FRP}{P_{f0}}\right)^{\gamma} \exp\left(-\delta N_{FT}^2 / N_0^2\right)$$

where H_P is height of plume top; H_{PBL} is PBL height; FRP is fire radiative power; P_{f0} is reference fire power; P_{f0} = 10^6 W; N_0 is the reference Brunt-Väisälä frequency; N_0^2 = 2.5×10^{-4} s^{-2}; N_{FT} is the Brunt-Väisälä frequency; α is the fraction of PBL passed freely; $\alpha < 1$; β is the weight of fire intensity contribution ($\beta > 0\, m$); γ is the power of dependence on FRP; $\gamma < 0.5$; δ is the weight of dependence on free troposphere stability ($\delta \geq 0$). The scheme provides two alternative ways of setting the $\alpha, \beta, \gamma, \delta$ parameters:

1. one-stage:

   H_{P1}: $\alpha = 0.24;\ \beta = 170m;\ \gamma = 0.35;\ \delta = 0.6$

2. two-stage:

   stage 1 (first guess):

   H_{P0}: $\alpha = 0.15;\ \beta = 102\, m;\ \gamma = 0.49;\ \delta = 0$

   stage 2 (using H_{P0} from stage 1):

   H_{P1}: $\alpha = 0.24;\ \beta = 170\, m;\ \gamma = 0.35;\ \delta = 0.6\ (H_{P0} \leq H_{pbl})$

   H_{P2}: $\alpha = 0.93;\ \beta = 298\, m;\ \gamma = 0.13;\ \delta = 0.7\ (H_{P0} > H_{pbl})$

N_{FT} can be derived from potential temperature (θ):

$$N_{FT} = \sqrt{\frac{g}{\theta}\frac{d\theta}{dz}}\ (z \approx 2H_{PBL})$$

The Sofiev parameterization therefore requires FRP, Brunt-Väisälä frequency (N_{FT}) and PBL height (H_{PBL}). While N_{FT} and H_{PBL} can be calculated from CAMx meteorological variables, GFAS1.2 is the only FEI that includes FRP.

2.2.4.2 Case Study Analysis of Sofiev Formulation and Modifications

To examine the relationship between FRP and Sofiev plume top height, we selected a case study centered on the Kincade Fire, the largest of California's 2019 fire season[11]. The GFAS grid cell centered on the fire on October 24, 2019 – the day after ignition – showed a daily FRP value of 35 W m^{-2}. For context, this FRP value is in the 99.9 percentile of all GFAS-detected fires across North America from April-Oct 2019. We selected a 12 km CAMx grid cell near the Kincade Fire to provide N_{FT} and PBL height (~1270 m) for the Sofiev algorithm at 2 PM PDT on October 24, 2019.

Using a box model, we calculated plume top heights for a range of different FRP values for the Sofiev 1-stage (red) and 2-stage (cyan) approaches in Figure 2-6. We plot the WRF PBL height (black) and PBL+500 m (blue) plume top height for reference. From this plot, we make the following observations:

1. Sofiev 1-stage and 2-stage H_p are identical for FRP values below 0.9 W m^{-2}
2. Sofiev 1-stage is confined to the PBL for all FRPs < 5.0 W m^{-2}
3. An abrupt transition in Sofiev 2-stage H_P occurs around 0.9 W m^{-2} when H_{P0} exceeds H_{PBL} (switches from H_{P1} to H_{P2} above)
4. Sofiev 2-stage H_P increases slowly above 0.9 W m^{-2} and is just below PBL+500 m at 100 W m^{-2}

To address the abrupt transition in Sofiev 2-stage when the first guess H_{P0} exceeds H_{PBL}, we developed an approach to smooth the transition with increasing FRP (green line in Figure 2-6; H_{P3} hereafter):

$$H_{P3} = H_{P1} \qquad (H_{P0} \leq 0.5\, H_{pbl})$$

$$H_{P3} = H_{P2} \qquad (H_{P0} \geq 1.5\, H_{pbl})$$

$$H_{P3} = (1-k)H_{P1} + kH_{P2} \qquad (0.5\, H_{PBL} \leq H_{P0} \leq 1.5\, H_{pbl})$$

$$\text{where: } k = (H_{P0}/H_{PBL}) - 0.5$$

We then explored the diurnal evolution of plume top heights for this new formulation. We again used the same CAMx grid cell, but calculated H_{P3} for each hour using hourly N_{FT} and PBL heights of October 24, 2019. Figure 2-7 shows H_{P3} in green, along with the WRF H_{PBL} (black) and PBL+500 m H_p (blue) for reference. This plot uses the daily average FRP from GFAS of 35 W m^{-2} from the Kincade Fire. The Sofiev parameterization is calibrated with MISR measurements, which have a local time overpass around 10 AM each day. It is therefore not designed to apply to nighttime conditions when PBL heights are often tens of meters deep. H_{P3} (and therefore the entire smoke column) is confined to the PBL during the early morning hours, which is not realistic for a fire of this intensity.

For intense fires like the Kincade Fire, we expect plume top heights to reach the free troposphere during all hours of the day. To allow plume top heights to better scale with fire intensity (higher FRP), especially during low-PBL nighttime hours, we further refined our plume top height (H_{P4}) defined as:

[11] https://www.fire.ca.gov/incidents/2019/10/23/kincade-fire

$$H_{P4} = H_{P3} \qquad (H_{P0} \leq H_{pbl})$$

$$H_{P4} = \max\left[H_{P1}, H_{P3,} H_{P0}/H_{PBL} + 100\right] \qquad (H_{P0} > H_{pbl})$$

Figure 2-8 shows this new plume top height for the same meteorological conditions as in Figure 2-7, but for a range of FRP values from 0.1 to 100 W m^{-2}. Using this definition of H_P, we find that smaller fires (FRP less than 0.1 W m^{-2}) have plume top heights that are entirely within the PBL during midday hours. Larger fires like Kincade extend well into the free troposphere. Overall, we expect that our modifications to the Sofiev scheme will produce more realistic plume top heights that are better correlated with fire intensity.

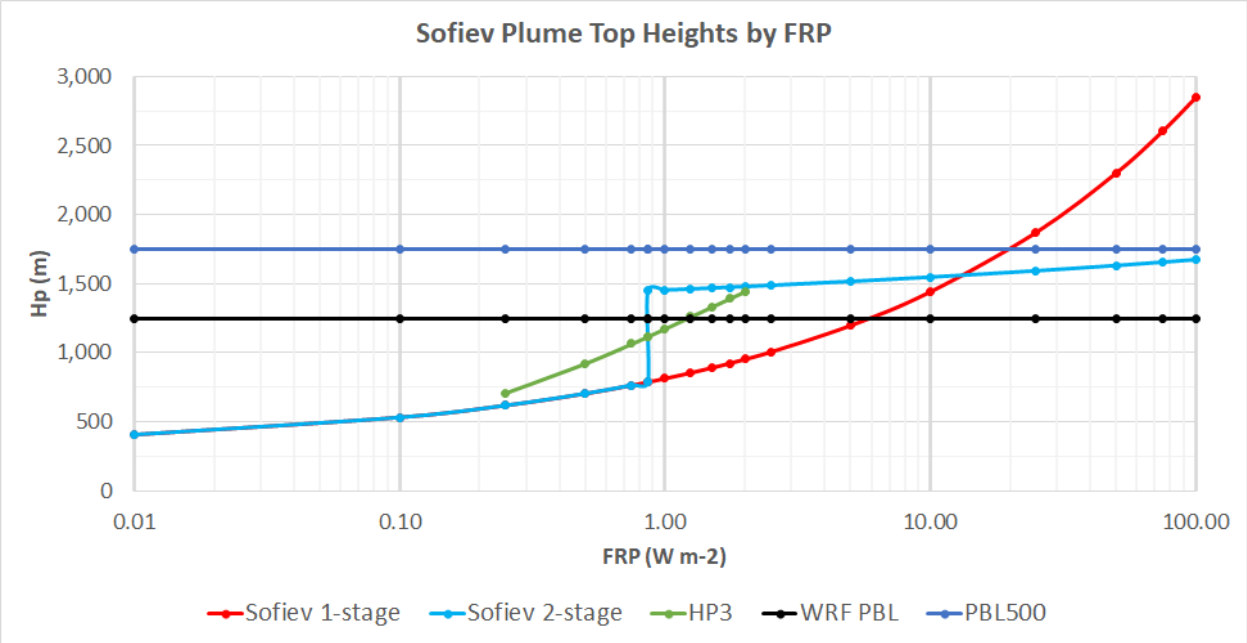

Figure 2-6. Sofiev 1-stage (red), Sofiev 2-stage (cyan), HP3 (green) and PBL500 (blue) plume top heights and WRF PBL height (black) for a grid cell in Sonoma County, CA on October 24, 2019 at 2 PM PDT.

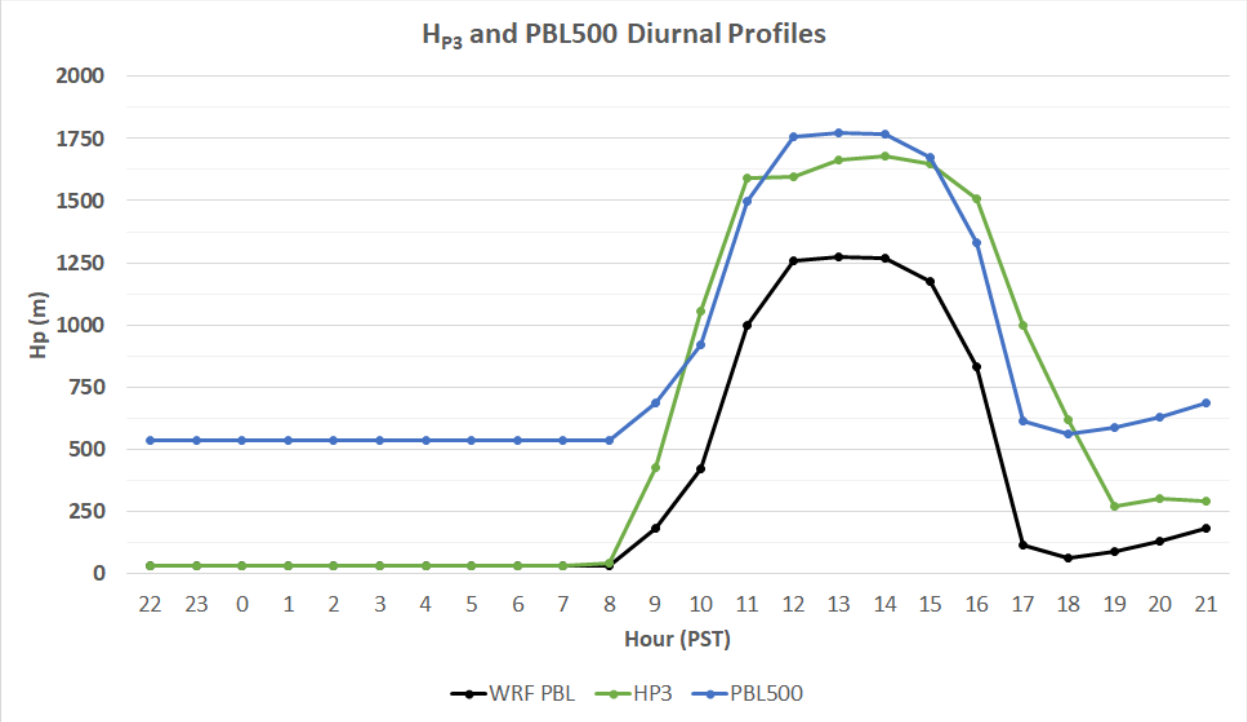

Figure 2-7. H_{P3} (green) and PBL500 (blue) plume top heights and WRF PBL heights (black) for a grid cell in Sonoma County, CA on October 24, 2019.

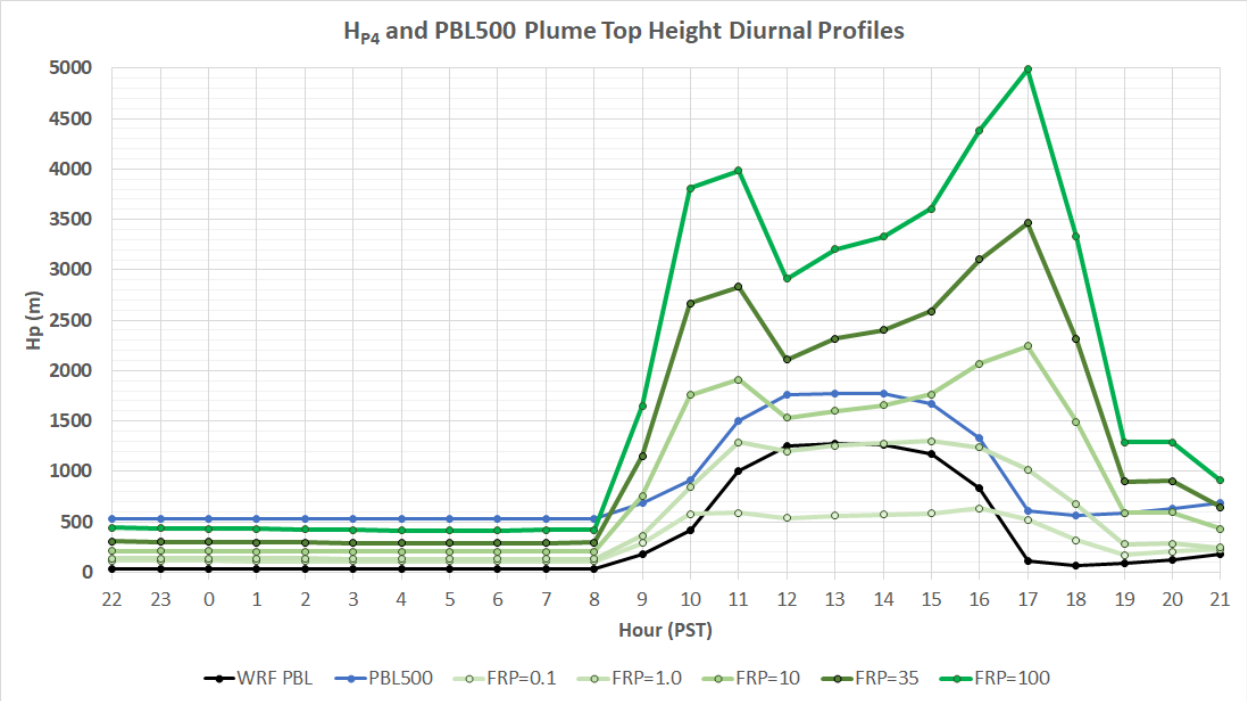

Figure 2-8. H_{P4} for FRP values of 0.1, 1.0, 10, 35 and 100 W m^{-2} (shades of green) and PBL500 (blue) plume top heights and WRF PBL heights (black) for a grid cell in Sonoma County, CA on October 24, 2019.

2.2.4.3 FRP Estimation for non-GFAS FEIs

As mentioned earlier, GFAS1.2 is the only FEI of the four FEIs that reports FRP, so we need to estimate FRP for the other three FEIs. We decided to explore relationships between FRP and CO emissions fluxes from GFAS to back calculate FRP for the other three FEIs. Examination of this relationship revealed distinct linear regression slopes that correspond to landcover-specific fuel types used by the GFAS system. We derived best-fit linear regressions for Western and Eastern U.S. regions (separated by -104° longitude) by RAVE landcover type. The slopes for these regression lines are shown in Table 2-6 along with correlation coefficients. In general, we found excellent agreement between CO and FRP by landcover type and region (East r: 0.89-1.00; West r: 0.95-1.00). However, we found considerable discrepancies within the forest landcover type and therefore decided to divide it into three distinct landcover types based on latitude of the corresponding GFAS grid cell, consistent with approaches defined in Andela et al. (2013) and van Leeuwen et al. (2014):

- Boreal Forest (north of 50° N)
- Temperate Forest (between 30° and 50° N)
- Tropical Forest (south of 30° N)

Figure 2-9 is an example scatter plot showing Western U.S. temperate forest daily FRP and CO emission fluxes for individual GFAS 0.1° grid cells. The resulting relationships among RAVE landcover types and CO:RFP slope shown in Table 2-6 are used to derive FRP from CO emission for all three other FEIs.

Table 2-6. CO:FRP factors by landcover type and North America region with correlation.

Region	Landcover Type	CO:FRP Factor	r
East	Boreal Forest (north of 50° N)	6.87	0.96
East	Temperate Forest (between 30° and 50° N)	2.36	0.84
East	Tropical Forest (south of 30° N)	4.21	0.93
East	Shrubland	6.73	1.00
East	Savanna	6.68	1.00
East	Grassland	5.68	0.95
East	Cropland	4.43	0.89
West	Boreal Forest (north of 50° N)	2.00	0.98
West	Temperate Forest (between 30° and 50° N)	6.74	0.98
West	Tropical Forest (south of 30° N)	6.74	1.00
West	Shrubland	1.97	1.00
West	Savanna	6.88	0.98
West	Grassland	8.94	0.95
West	Cropland	9.83	0.95

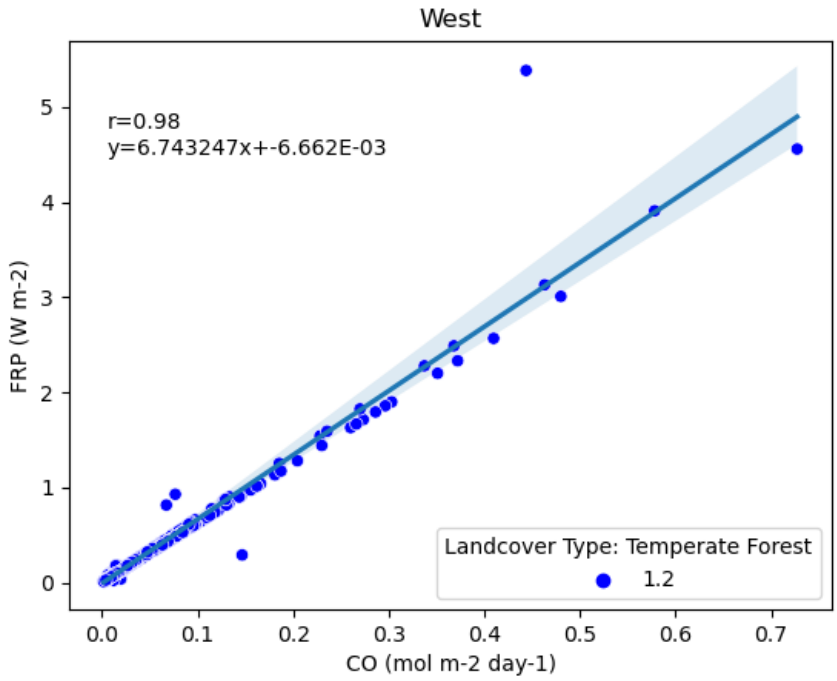

Figure 2-9. Monthly scatter plot showing daily FRP (W m^{-2}) and CO emissions fluxes (mol m^{-2} day^{-1}) for the Western US in April-May 2019 for temperate forest landcover type.

3.0 FEI CAMX SIMULATION MODEL PERFORMANCE EVALUATION

3.1 CAMx Model Configuration and FEI Sensitivity Tests

3.1.1 CAMx Configuration

TCEQ's 2019 CAMx modeling showed large positive ozone biases related to FINN fire emissions throughout April and May of 2019, when transport of smoke from biomass burning in Mexico and Central America was frequent. As decided in consultation with TCEQ staff, Ramboll ran CAMx for the April 1 through May 31, 2019 period on a two-way nested grid system comprising a North American domain (36 km grid spacing), US domain (12 km grid spacing), and East Texas domain (4 km grid spacing). Figure 3-1 presents the nesting arrangement for these grids, Figure 3-2 shows detail for the East Texas domain, and Figure 3-3 shows the vertical grid structure.

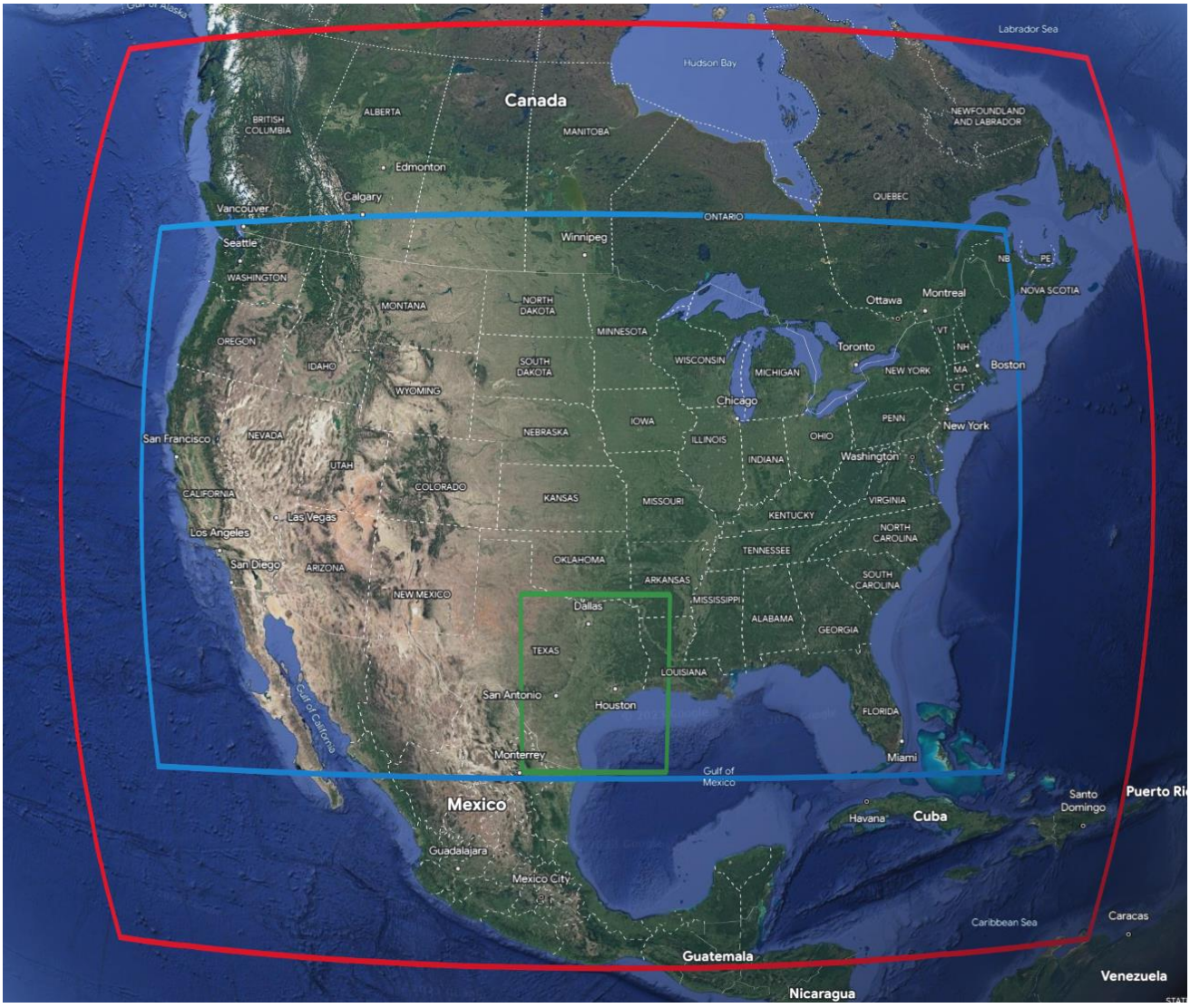

Figure 3-1. Nested grid domains in the TCEQ 2019 modeling platform.

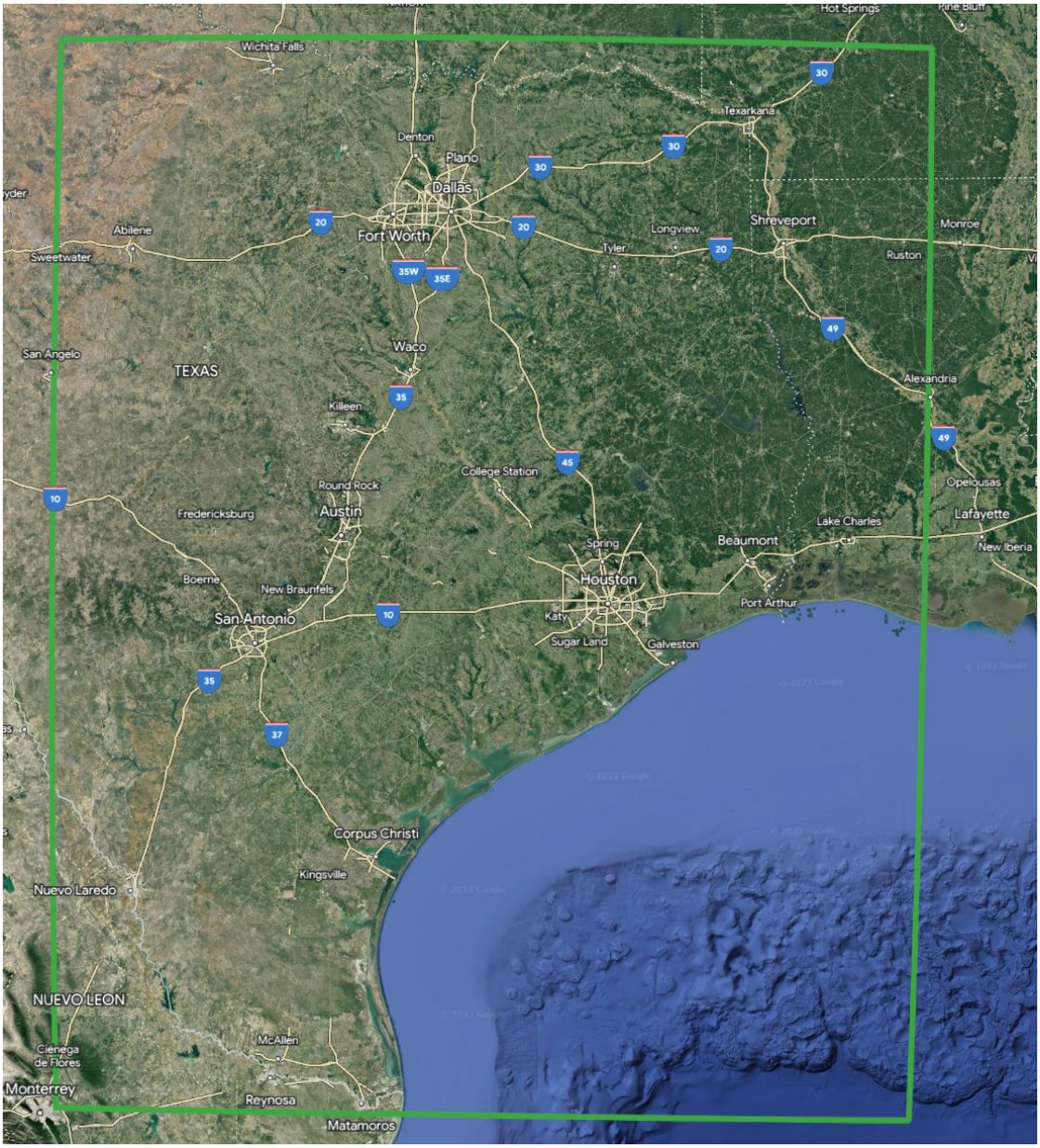

Figure 3-2. Coverage of the East Texas 4 km nested grid in the TCEQ 2019 modeling platform.

2019 APR-OCT (txs_4km domain)

WRF Layer	CAMx Layer	Top (m AGL)	Center (m AGL)	Thickness (m)
42	30	18238	16435	3606
39	29	14632	13173	2919
36	28	11713	10757	1913
34	27	9801	8968	1665
32	26	8135	7472	1326
30	25	6810	6266	1087
28	24	5722	5268	909
26	23	4813	4428	770
24	22	4044	3686	715
22	21	3329	3159	340
21	20	2989	2825	329
20	19	2661	2502	319
19	18	2342	2213	258
18	17	2084	1958	252
17	16	1832	1709	246
16	15	1586	1465	241
15	14	1345	1274	142
14	13	1203	1133	140
13	12	1063	994	138
12	11	925	856	137
11	10	788	743	90
10	9	698	653	90
9	8	608	564	89
8	7	519	475	88
7	6	431	387	88
6	5	344	300	87
5	4	257	214	86
4	3	170	128	86
3	2	85	59	51
2	1	34	17	34

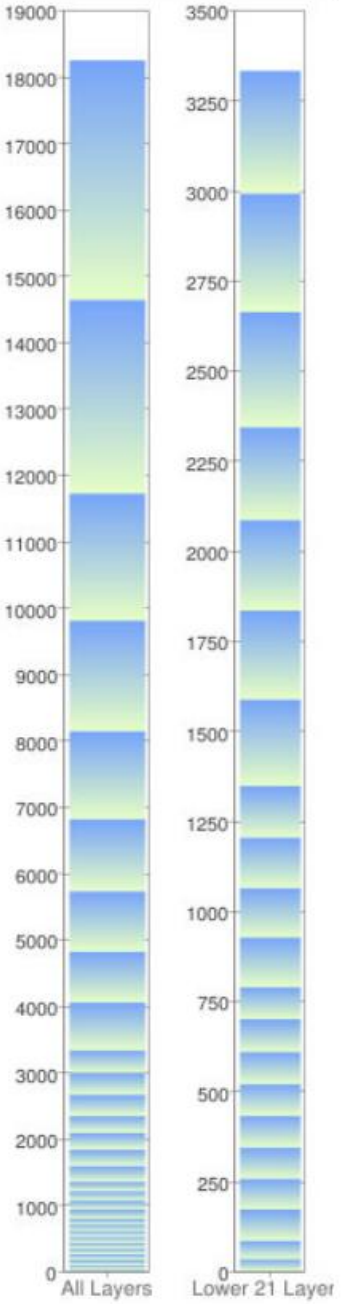

Figure 3-3. Vertical grid structure for all CAMx nested grid domains in the TCEQ 2019 modeling platform.

The TCEQ provided the following 2019 modeling platform datasets for this project:

- All CAMx-ready gridded and point anthropogenic and biogenic emission input files for all grids;

- All CAMx-ready meteorological input files for all grids derived using the Weather Research and Forecasting model (WRF; Skamarock et al., 2021);
- All CAMx-ready ancillary input files (initial/boundary/top conditions, photolysis rates, ozone column map).

The TCEQ also provided example model configuration files and scripts to facilitate Ramboll's model setup. Table 3-1 lists the CAMx configuration for the tests described in this Section.

Table 3-1. CAMx model configuration for tests using the TCEQ 2019 modeling platform.

Model Options/Settings	CAMx Configuration
Version	v7.20
Date Range	April 1 – May 31, 2019
Time Zone	Central Standard Time (CST)
Map Projection	Lambert Conic Conformal
2-Way Nested Grid System	36/12/4 km (East Texas) horizontal grid resolution, 30 vertical layers up to ~20 km
Horizontal Advection	PPM
Vertical Advection	IMPLICIT
Gas-Phase Chemistry	CB6r5
Particulate Chemistry	CF2
Chemistry Solver	EBI
Dry Deposition	WESELY89
Plume-in-Grid	Off
Bi-directional Ammonia	Off
Wet Deposition	On
ACM2 Boundary Layer Diffusion	Off
Surface Chemistry Model	Off
Inline Ix Emissions	On
Super Stepping	On
3-D Output	On (4 km grid only)

3.1.2 FEI Sensitivity Tests

Seven sensitivity runs were conducted in two phases, shown in Table 3-2. Other than changing FEI and temporal/vertical emission allocation schemes, all other inputs and model settings were identical among all seven runs conducted for this project. In phase 1, four runs were conducted using each of the FEIs (FINN2.5, GFAS1.2, QFED2.5, and FEER1.0). Each of these sensitivity tests used the RAVE temporal and Sofiev vertical allocation schemes. In phase 2, we ran four CAMx sensitivity tests for the best performing FEI from phase 1 (GFAS1.2) to examine impacts from all four possible combinations of FEI temporal and vertical allocation schemes (where one of these four sensitivity tests, run2, was run in phase 1).

Table 3-2. CAMx model configuration for FEI sensitivity tests.

CAMx Test	FEI Input	Temporal Scheme	Vertical Scheme
run1	FINN2.5	RAVE	Sofiev
run2	GFAS1.2	RAVE	Sofiev
run3	QFED2.5	RAVE	Sofiev
run4	FEER1.0	RAVE	Sofiev
run5	GFAS1.2	RAVE	PBL500
run6	GFAS1.2	Default	PBL500
run7	GFAS1.2	Default	Sofiev

3.2 Model Performance Evaluation

As decided in consultation with TCEQ, we evaluated model performance by analyzing modeled maximum daily average 8-hour (MDA8) ozone statistics on a region-wide basis across all Continuous Ambient Monitoring Stations (CAMS) within each of the Dallas-Fort Worth (20 sites), San Antonio (12 sites) and Houston-Galveston-Brazoria (38 sites) regions. In addition, we performed a detailed ozone model performance evaluation at the six CAMS shown in Table 3-3 using statistical analyses and time series. TCEQ chose the three CAMS in San Antonio as these are all the regulatory monitors within Bexar County. TCEQ selected Grapevine Fairway C70, Dallas Executive Airport C402, and Denton Airport North C56 to represent a sample of different locations in the Dallas-Fort Worth region. We also compared hourly modeled $PM_{2.5}$ against CAMS observations in each of the three regions using time series only. We did not calculate $PM_{2.5}$ model performance statistics because the TCEQ emissions inventory does not contain PM for the onroad sector.

Table 3-3. CAMS selected for detailed ozone model performance evaluation.

Monitor Name	CAMS ID	Area
Camp Bullis C58	BOER	San Antonio
Calaveras Lake C59	CALA	San Antonio
San Antonio Northwest C23	SAWC	San Antonio
Grapevine Fairway C70	GRAP	Dallas-Fort Worth
Dallas Executive Airport C402	REDB	Dallas-Fort Worth
Denton Airport North C56	DENN	Dallas-Fort Worth

3.2.1 Phase 1 Comparison

Error! Reference source not found., **Error! Reference source not found.**, and **Error! Reference source not found.** provide MDA8 ozone statistics for the Dallas-Fort Worth, San Antonio, and Houston regions during April 6 – May 31, 2019, respectively. The best performing run (lowest bias and error, highest R^2, etc.) in each region is shown in bold text. For the Dallas-Fort Worth region, the FINN2.5 run shows the smallest normalized mean bias (NMB: +1.4%) of the four runs, but it also has the largest normalized mean error (NME: 17.4%). Further, the FINN2.5 run has substantially lower correlation (R^2: 0.194) than the other three runs (FEER1.0: 0.423; GFAS1.2 and QFED2.5: 0.462). In the San Antonio and Houston regions, all four runs display a positive bias, with FINN2.5 showing substantially higher bias (San Antonio NMB: +24.8%; HGB NMB: +10.0%) and error (San Antonio NME: 30.9%; HGB NME: 22.6%) compared to the other three sensitivity runs (San Antonio: 7.8% to 13.0%; HGB: 2.6% to 5.3%). As in the Dallas-Fort Worth region, FINN2.5 displays substantially lower correlation (San Antonio R^2: 0.053; HGB R^2: 0.348) compared to the other three runs (San Antonio R^2: 0.314 to 0.410; HGB R^2: 0.490 for GFAS1.2, QFED2.5 and FEER1.0). While bias and error

statistics among the GFAS1.2, QFED2.5 and FEER1.0 runs are similar for San Antonio and Houston, GFAS1.2 shows slightly lower bias and error compared to other two runs.

The next set of tables provide the same MDA8 ozone statistics as in the previous tables but for individual CAMS in the San Antonio region: Camp Bullis C58 (BOER; **Error! Reference source not f ound.**), Calaveras Lake C59 (CALA; **Error! Reference source not found.**) and San Antonio Northwest C23 (SAWC; **Error! Reference source not found.**). At all three CAMS, FINN2.5 displays c onsiderably higher NME (22.8% to 28.4%) than the other three runs (13.3% to 18.0%). Similarly, FINN2.5 shows the highest absolute value of NMB at the three San Antonio CAMS (+12.0% to +22.6%) compared to the other three runs (-4.4% to +10.7%). FINN2.5 also shows substantially worse correlation (R^2: 0.029 to 0.078) compared to the other three runs (R^2: 0.336 to 0.562).

Similar to the previous set of tables, Table 3-10, Table 3-11, and Table 3-12 provide site-specific MDA8 ozone statistics at Grapevine Fairway C70 (GRAP), Dallas Redbird Airport C402 (REDB) and Denton Airport South C56 (DENN) CAMS, respectively, in the Dallas-Fort Worth region. FINN2.5 shows the lowest absolute value of NMB at the REDB (-0.9%) and DENN (+0.9%) CAMS, but the highest absolute value of NMB at GRAP (+6.0%). FINN2.5 displays the highest error at all three CAMS, ranging from 16.4% at REDB to 18.1% at GRAP. As shown in XXX and XXX correlation is again substantially lower for FINN2.5 (R^2: 0.152 to 0.221) compared to the other three runs (R^2: 0.410 to 0.548) at the Dallas-Fort Worth CAMS.

Overall, the region-wide and site-specific statistics calculated across the entire April 6 – May 31, 2019 modeling episode show that the FINN2.5 run exhibits the poorest statistical performance of the four runs. Performance is similar among the other three runs (GFAS1.2, QFED2.5 and FEER1.0) and substantially better than FINN2.5. We examine hourly ozone and $PM_{2.5}$ time series below to better understand the variation between the four sensitivity runs.

Figure 3-4 shows hourly ozone (top panel), ozone bias (2nd panel from top), $PM_{2.5}$ (3rd panel from top) and $PM_{2.5}$ bias (bottom panel) time series at San Antonio Northwest C23 for April 2019. Grey shaded regions represent days where TCEQ's modeling exhibited poor ozone performance (April 6-7, 13 and 23) associated with FINN fire emissions. In agreement with TCEQ's modeling, FINN2.5 shows substantial positive midday peak ozone biases of up to 40 ppb. The other three FEIs show lower biases on these days. FINN2.5 overestimates $PM_{2.5}$ by nearly 60 ug m^{-3} on April 23, while the other 3 FEIs agree better with observations on this day.

Figure 3-5 shows the same time series as in Figure 3-4 but for May 2019. Similar to the previous plot, we find frequent large ozone overestimates for FINN2.5, particularly on May 6, 7, and 22. On each of these days, GFAS1.2, QFED2.5, and FEER1.0 all show substantially lower biases. The $PM_{2.5}$ time series show that FINN2.5 appears to match some of the highest observed peaks (May 9 and 22) better than the other three FEIs. However, the incomplete PM emissions inventory may be masking an otherwise substantial bias in the FINN run. Another feature apparent in the $PM_{2.5}$ time series is more separation between the GFAS1.2, QFED2.5 and FEER1.0 runs compared to the ozone results. We provide similar ozone and $PM_{2.5}$ time series for Calaveras Lake C59 in Appendix A.

Figure 3-6 shows April 2019 hourly ozone (top panel), ozone bias (2nd panel from top) and May 2019 hourly ozone (3rd panel from top) and ozone bias (bottom panel) time series at Denton Airport South C56. All runs show ozone underpredictions for most days in April. The ozone overpredictions on several days across all FEIs tend to cancel out these underpredictions, leading to low hourly ozone NMB for all runs (-4.2% to +0.5%). NME is substantially higher (21.1% to 23.3%), reflecting the mix of negative and positive biases across the month. While FINN2.5 again shows high positive bias on

several days (April 7, 23 and 30), the other three FEIs also show lower and similar biases on these days. The time series at this site and others in the Dallas-Fort Worth region (shown in Appendix A) display more spread among the GFAS1.2, QFED2.5 and FEER1.0 runs as compared to San Antonio CAMS. For example, on April 9, FEER1.0 midday peak ozone is about 10 ppb greater than QFED2.5. This day is an example where FINN2.5 shows one of the lowest ozone concentrations (similar to GFAS1.2) of the four FEIs. The May 2019 ozone time series (see bottom two panels of Figure 3-6) show large midday peak ozone overpredictions from FINN2.5 on May 20 (over 20 ppb) and May 22 (over 40 ppb). The other three FEIs show smaller positive ozone biases on these days. We provide similar ozone time series for Camp Bullis C58, Grapevine Fairway C70, and Dallas Redbird Airport C402 in Appendix A.

We generated hourly ozone concentration maps for the CAMx 36 km domain for the 2-month episode. Figure 3-7 shows the 36 km ozone map for April 6, 2019 at 1 PM CST. Ozone concentrations in Southern Mexico and Guatemala (over 140 ppb) indicate much more widespread and intense fire activity in FINN2.5 (top left of Figure 3-7) as compared to the other three FEIs. We find that FINN2.5 consistently displays substantially higher ozone concentrations in Southern Mexico and Central America throughout the 2-month episode.

Figure 3-8 shows a similar map for April 9, 2019 at 3 PM CST. This plot shows ozone greater than 70 ppb in Eastern Nebraska from fire activity for all four of the FEIs. Figure 3-9 shows a map of NOAA HMS fires, with a large concentration of fire detects in Eastern Nebraska. FEER1.0 shows the highest ozone concentrations (above 120 ppb) in this region, which are then transported into Dallas. This explains the discrepancy between the other three FEIs on this day in the Dallas-Fort Worth ozone time series (see Figure 3-6 and Appendix A).

Figure 3-10 shows the 36 km hourly ozone concentration map for May 30, 2019 at 4 PM CST. All four FEIs show ozone peaks in the vicinity of the Northern Alberta wildfires[12]. The magnitude of ozone concentrations varies substantially between the FEIs. GFAS1.2 has the highest ozone concentration at 186 ppb, while QFED2.5 has the lowest (about 60 ppb). FINN2.5 (~120 ppb) and FEER1.0 (~100 ppb) are in between these two extremes.

Overall, we conclude that FINN2.5 results in large frequent ozone overpredictions throughout the modeling episode while the other three FEIs (GFAS1.2, QFED2.5 and FEER1.0) generally agree better with observations. While FINN2.5 does exhibit some $PM_{2.5}$ overpredictions compared to observations, the current modeling platform contains an incomplete emission inventory for PM and therefore we cannot conduct a complete model evaluation for FEI impacts on $PM_{2.5}$. The FINN2.5 FEI uses a burned area approach, while GFAS1.2, QFED2.5 and FEER1.0 FEIs use a fire radiative power (FRP) approach to estimate fire emissions. Therefore, it is not surprising that the FINN2.5 run shows substantially different ozone and $PM_{2.5}$ concentrations compared to the other three FEI runs. The differences between these three FRP-based FEIs are small on most days and the differences in statistical performance may not be significant enough to determine a clear winner. We choose GFAS1.2 due to a combination of good overall performance and because it explicitly reports helpful parameters like FRP and vertical plume heights. Since our modeling episode covers only two months, we cannot suggest a particular FEI for different modeling episodes or applications.

[12] https://www.nasa.gov/image-feature/goddard/2019/alberta-canada-experiencing-an-extreme-fire-season

Table 3-4. MDA8 ozone statistics for the Dallas-Fort Worth TCEQ Region during the April 6 – May 31, 2019 period for each FEI sensitivity test.

MDA8 Ozone Statistics	FINN2.5	GFAS1.2	QFED2.5	FEER1.0
Number of Observations	1066	1066	1066	1066
Mean Concentration – Observations (ppb)	44.2	44.2	44.2	44.2
Mean Concentration – Model (ppb)	44.8	41.9	42.2	43.5
R^2	0.194	**0.462**	**0.462**	0.423
Mean Bias (ppb)	**0.6**	-2.3	-2.0	-0.7
Mean Error (ppb)	7.7	6.7	6.6	6.7
Normalized Mean Bias (%)	**1.4**	-5.2	-4.5	-1.6
Normalized Mean Error (%)	17.4	15.2	**15.0**	15.1
Mean Fractional Bias (%)	2.7	-3.8	-3.1	**-0.3**
Mean Fractional Error (%)	17.9	16.2	16.0	**15.9**

Table 3-5. MDA8 ozone statistics for the San Antonio TCEQ Region during the April 6 – May 31, 2019 period for each FEI sensitivity test.

MDA8 Ozone Statistics	FINN2.5	GFAS1.2	QFED2.5	FEER1.0
Number of Observations	658	658	658	658
Mean Concentration – Observations (ppb)	38.9	38.9	38.9	38.9
Mean Concentration – Model (ppb)	48.5	41.9	42.5	43.9
R^2	0.053	**0.410**	0.397	0.314
Mean Bias (ppb)	9.6	**3.0**	3.6	5.1
Mean Error (ppb)	12.0	**7.0**	7.3	8.2
Normalized Mean Bias (%)	24.8	**7.8**	9.2	13.0
Normalized Mean Error (%)	30.9	**18.1**	18.6	21.1
Mean Fractional Bias (%)	23.9	**9.9**	11.3	14.7
Mean Fractional Error (%)	28.7	**18.9**	19.4	21.6

Table 3-6. MDA8 ozone statistics for the Houston TCEQ Region during the April 6 – May 31, 2019 period for each FEI sensitivity test.

MDA8 Ozone Statistics	FINN2.5	GFAS1.2	QFED2.5	FEER1.0
Number of Observations	1943	1943	1943	1943
Mean Concentration – Observations (ppb)	40.6	40.6	40.6	40.6
Mean Concentration – Model (ppb)	44.7	41.7	41.9	42.8
R^2	0.348	**0.490**	**0.490**	**0.490**
Mean Bias (ppb)	4.1	**1.1**	1.3	2.2
Mean Error (ppb)	9.2	**7.7**	7.7	7.9
Normalized Mean Bias (%)	10.0	**2.6**	3.3	5.3
Normalized Mean Error (%)	22.6	**18.8**	18.9	19.5
Mean Fractional Bias (%)	13.0	**6.3**	6.9	8.9
Mean Fractional Error (%)	23.7	**20.2**	20.4	21.0

Table 3-7. MDA8 ozone statistics at the Camp Bullis C58 (BOER) site in San Antonio region during April 6 – May 31, 2019 period for each FEI sensitivity test.

MDA8 Ozone Statistics	FINN2.5	GFAS1.2	QFED2.5	FEER1.0
Number of Observations	55	55	55	55
Mean Concentration – Observations (ppb)	44.0	44.0	44.0	44.0
Mean Concentration – Model (ppb)	49.8	43.2	43.7	45.2
R^2	0.078	**0.562**	0.548	0.436
Mean Bias (ppb)	5.8	-0.9	**-0.3**	1.2
Mean Error (ppb)	10.0	5.9	**5.9**	6.6
Normalized Mean Bias (%)	13.2	-2.0	**-0.7**	2.7
Normalized Mean Error (%)	22.8	13.4	**13.3**	14.9
Mean Fractional Bias (%)	13.5	**-0.5**	0.8	4.3
Mean Fractional Error (%)	21.8	14.1	**14.0**	15.5

Table 3-8. MDA8 ozone statistics at theCalaveras Lake C59 (CALA) site in San Antonio region during April 6 – May 31, 2019 period for each FEI sensitivity test.

MDA8 Ozone Statistics	FINN2.5	GFAS1.2	QFED2.5	FEER1.0
Number of Observations	55	55	55	55
Mean Concentration – Observations (ppb)	43.2	43.2	43.2	43.2
Mean Concentration – Model (ppb)	48.4	41.3	41.9	43.5
R^2	0.029	**0.490**	0.462	0.336
Mean Bias (ppb)	5.2	-1.9	-1.3	**0.3**
Mean Error (ppb)	10.2	**5.9**	6.0	6.8
Normalized Mean Bias (%)	12.0	-4.4	-3.0	**0.7**
Normalized Mean Error (%)	23.6	**13.7**	13.8	15.7
Mean Fractional Bias (%)	12.1	-3.2	**-1.7**	2.0
Mean Fractional Error (%)	22.2	**13.8**	14.0	15.9

Table 3-9. MDA8 ozone statistics at the San Antonio Northwest C23 (SAWC) site in San Antonio region during April 6 – May 31, 2019 period for each FEI sensitivity test.

MDA8 Ozone Statistics	FINN2.5	GFAS1.2	QFED2.5	FEER1.0
Number of Observations	55	55	55	55
Mean Concentration – Observations (ppb)	40.6	40.6	40.6	40.6
Mean Concentration – Model (ppb)	49.8	42.8	43.4	44.9
R^2	0.063	**0.504**	0.490	0.384
Mean Bias (ppb)	9.2	**2.2**	2.8	4.3
Mean Error (ppb)	11.5	**6.3**	6.5	7.3
Normalized Mean Bias (%)	22.6	**5.5**	6.9	10.7
Normalized Mean Error (%)	28.4	**15.5**	15.9	18.0
Mean Fractional Bias (%)	21.6	**7.2**	8.6	12.1
Mean Fractional Error (%)	26.4	**16.2**	16.6	18.5

Table 3-10. MDA8 ozone statistics at Grapevine Fairway C70 (GRAP) site during April 6 – May 31, 2019 period for each FEI sensitivity test.

MDA8 Ozone Statistics	FINN2.5	GFAS1.2	QFED2.5	FEER1.0
Number of Observations	55	55	55	55
Mean Concentration – Observations (ppb)	42.9	42.9	42.9	42.9
Mean Concentration – Model (ppb)	45.5	42.5	42.8	44.2
R^2	0.152	**0.436**	**0.436**	0.397
Mean Bias (ppb)	2.6	-0.5	**-0.1**	1.2
Mean Error (ppb)	7.8	6.2	**6.1**	6.6
Normalized Mean Bias (%)	6.0	-1.1	**-0.3**	2.9
Normalized Mean Error (%)	18.1	14.4	**14.2**	15.3
Mean Fractional Bias (%)	6.8	**0.2**	1.0	3.9
Mean Fractional Error (%)	18.4	15.4	**15.2**	16.0

Table 3-11. MDA8 ozone statistics at Dallas Redbird Airport Executive C402 (REDB) site during April 6 – May 31, 2019 period for each FEI sensitivity test.

MDA8 Ozone Statistics	FINN2.5	GFAS1.2	QFED2.5	FEER1.0
Number of Observations	55	55	55	55
Mean Concentration – Observations (ppb)	45.7	45.7	45.7	45.7
Mean Concentration – Model (ppb)	45.2	42.5	42.7	44.1
R^2	0.221	**0.548**	**0.548**	0.490
Mean Bias (ppb)	**-0.4**	-3.2	-2.9	-1.6
Mean Error (ppb)	7.5	6.6	**6.5**	6.5
Normalized Mean Bias (%)	**-0.9**	-7.0	-6.4	-3.4
Normalized Mean Error (%)	16.4	14.5	**14.3**	**14.3**
Mean Fractional Bias (%)	**0.4**	-5.9	-5.2	-2.3
Mean Fractional Error (%)	17.1	15.5	15.3	**15.2**

Table 3-12. MDA8 ozone statistics at Denton Airport South C56 (DENN) site during April 6 – May 31, 2019 period for each FEI sensitivity test.

MDA8 Ozone Statistics	FINN2.5	GFAS1.2	QFED2.5	FEER1.0
Number of Observations	55	55	55	55
Mean Concentration – Observations (ppb)	44.9	44.9	44.9	44.9
Mean Concentration – Model (ppb)	45.3	42.4	42.7	44.0
R^2	0.176	**0.449**	**0.449**	0.410
Mean Bias (ppb)	**0.4**	-2.5	-2.1	-0.9
Mean Error (ppb)	7.9	6.8	**6.7**	6.8
Normalized Mean Bias (%)	**0.9**	-5.5	-4.8	-2.0
Normalized Mean Error (%)	17.6	15.1	**14.9**	15.0
Mean Fractional Bias (%)	1.8	-4.4	-3.6	**-0.9**
Mean Fractional Error (%)	18.0	16.1	**15.9**	**15.9**

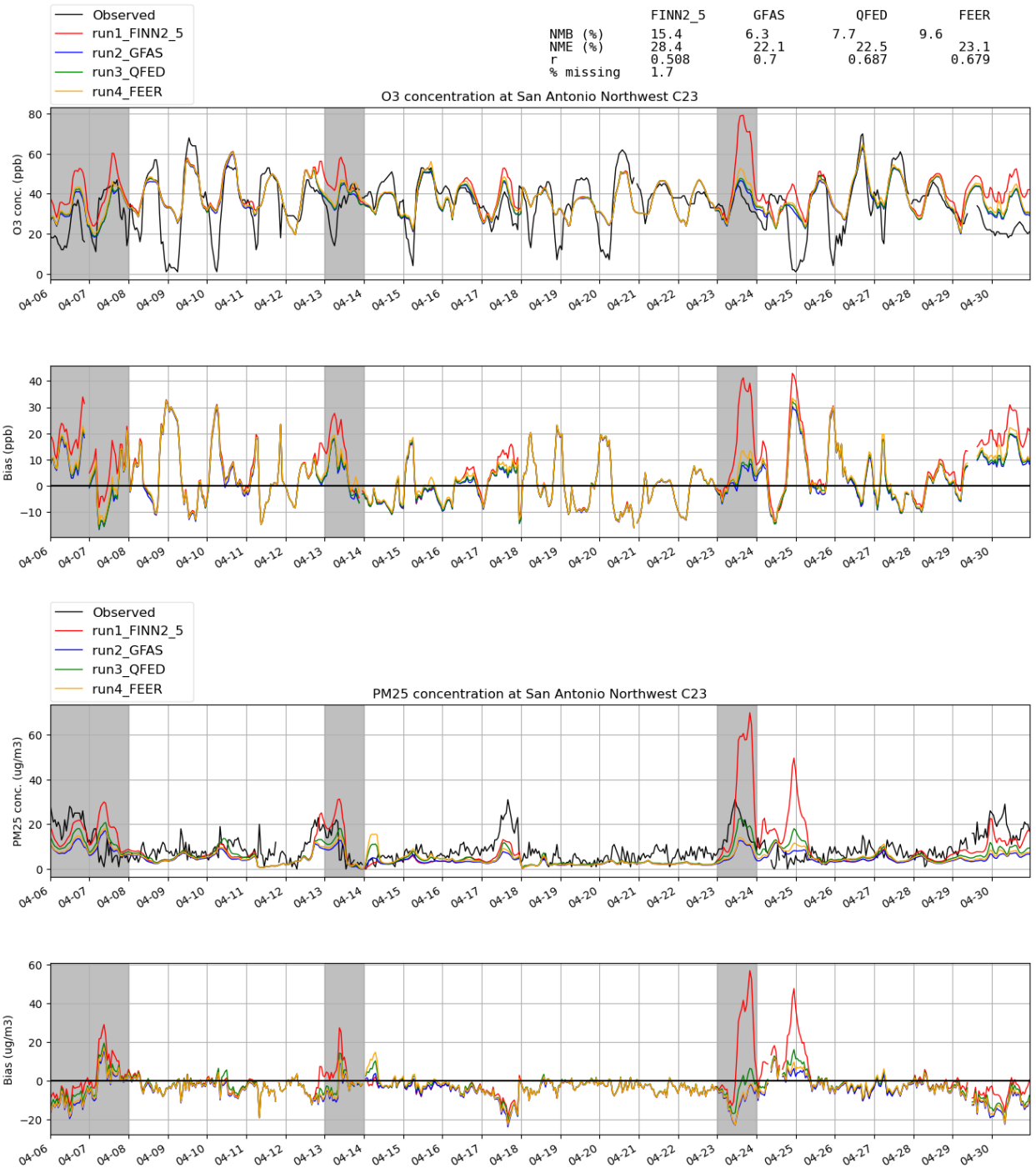

Figure 3-4. Hourly ozone (top panel), ozone bias (2nd panel from top), $PM_{2.5}$ (3rd panel from top) and $PM_{2.5}$ bias (bottom panel) time series at San Antonio Northwest C23 for April 2019. Grey shaded regions represent days when TCEQ's modeling exhibited poor ozone performance.

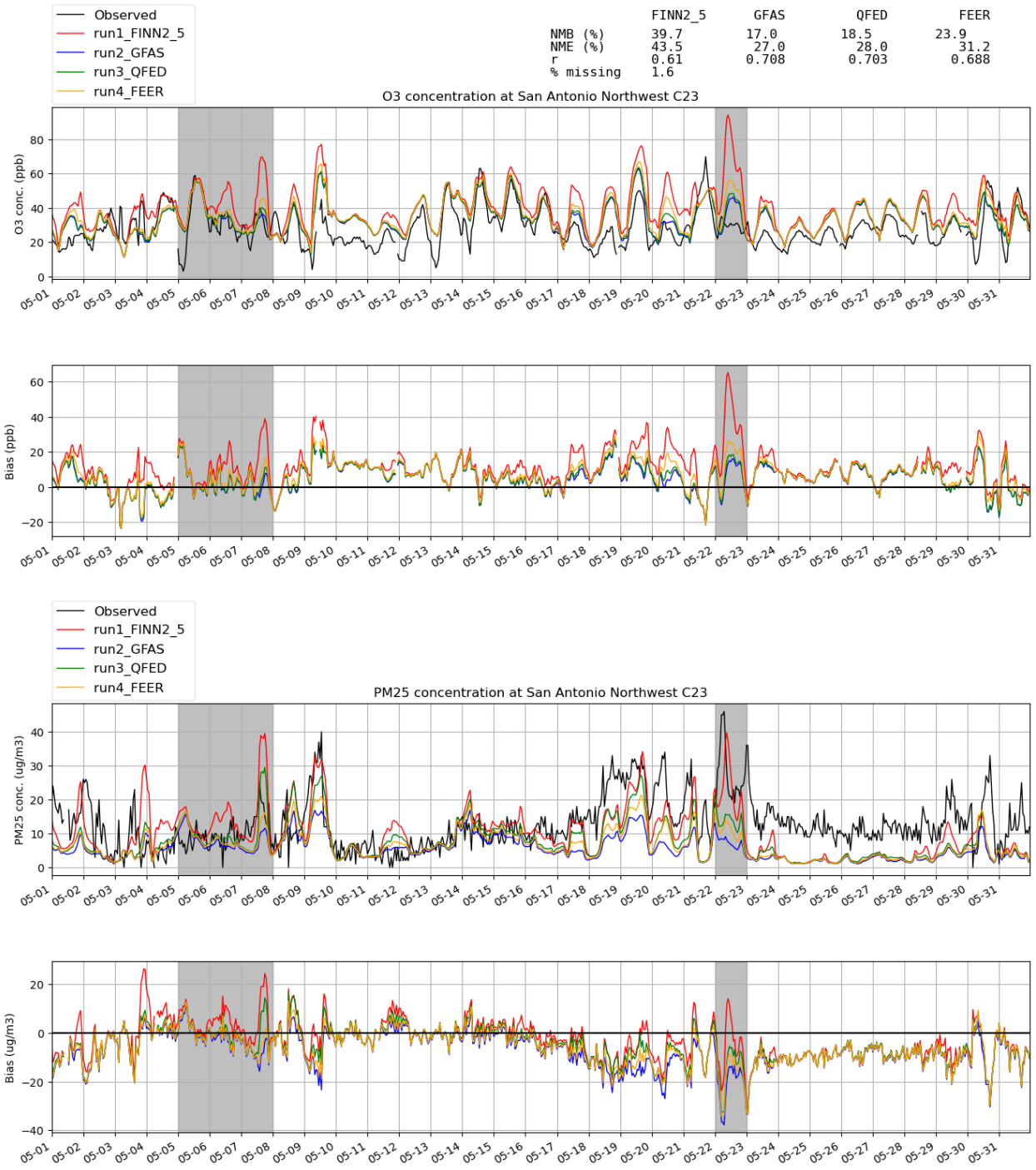

Figure 3-5. Hourly ozone (top panel), ozone bias (2nd panel from top), $PM_{2.5}$ (3rd panel from top) and $PM_{2.5}$ bias (bottom panel) time series at San Antonio Northwest C23 for May 2019. Grey shaded regions represent days when TCEQ's modeling exhibited poor ozone performance.

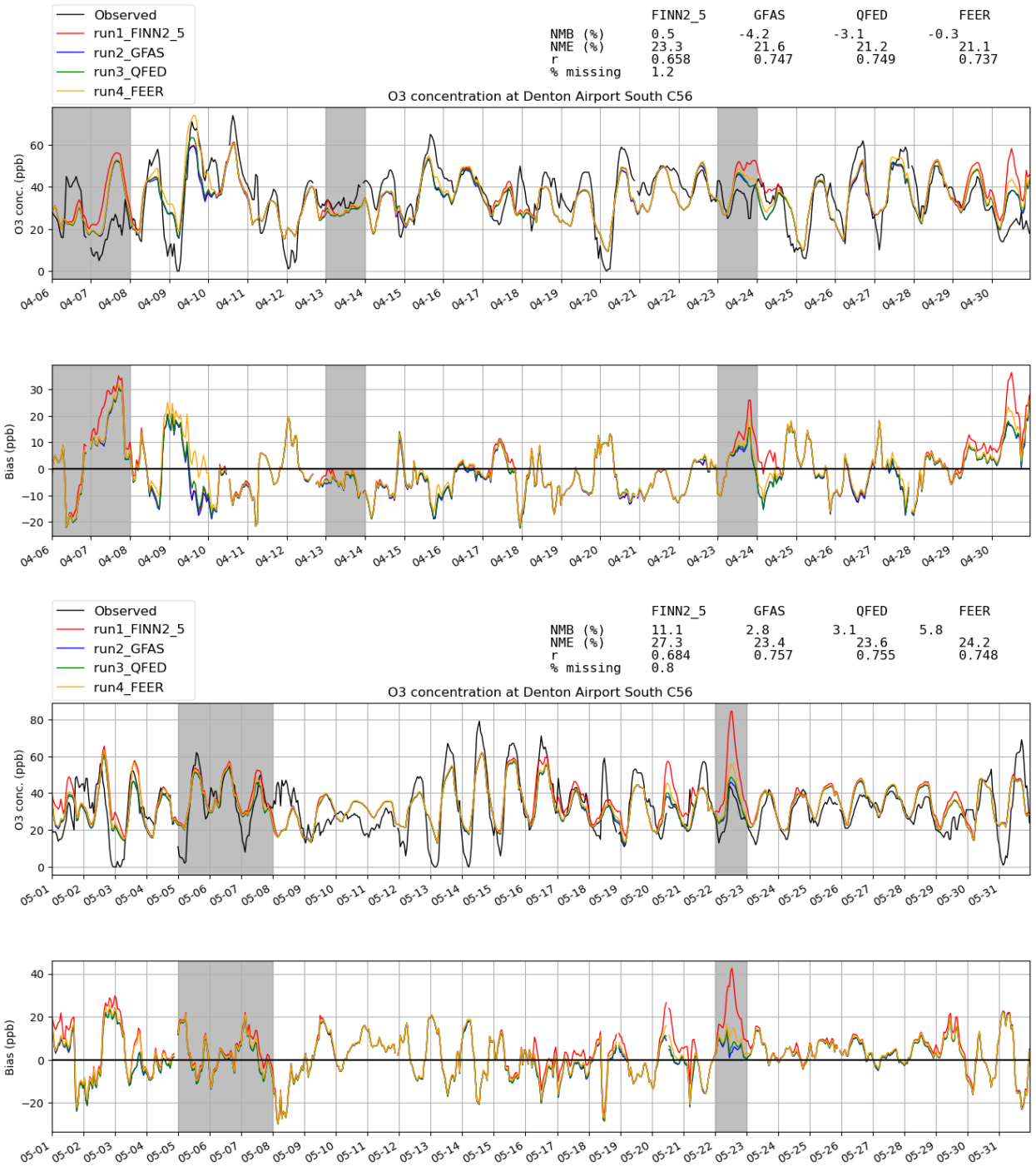

Figure 3-6. April 2019 hourly ozone (top panel), ozone bias (2nd panel from top) and May 2019 hourly ozone (3rd panel from top) and ozone bias (bottom panel) time series at Denton Airport South C56. Grey shaded regions represent days when TCEQ's modeling exhibited poor ozone performance.

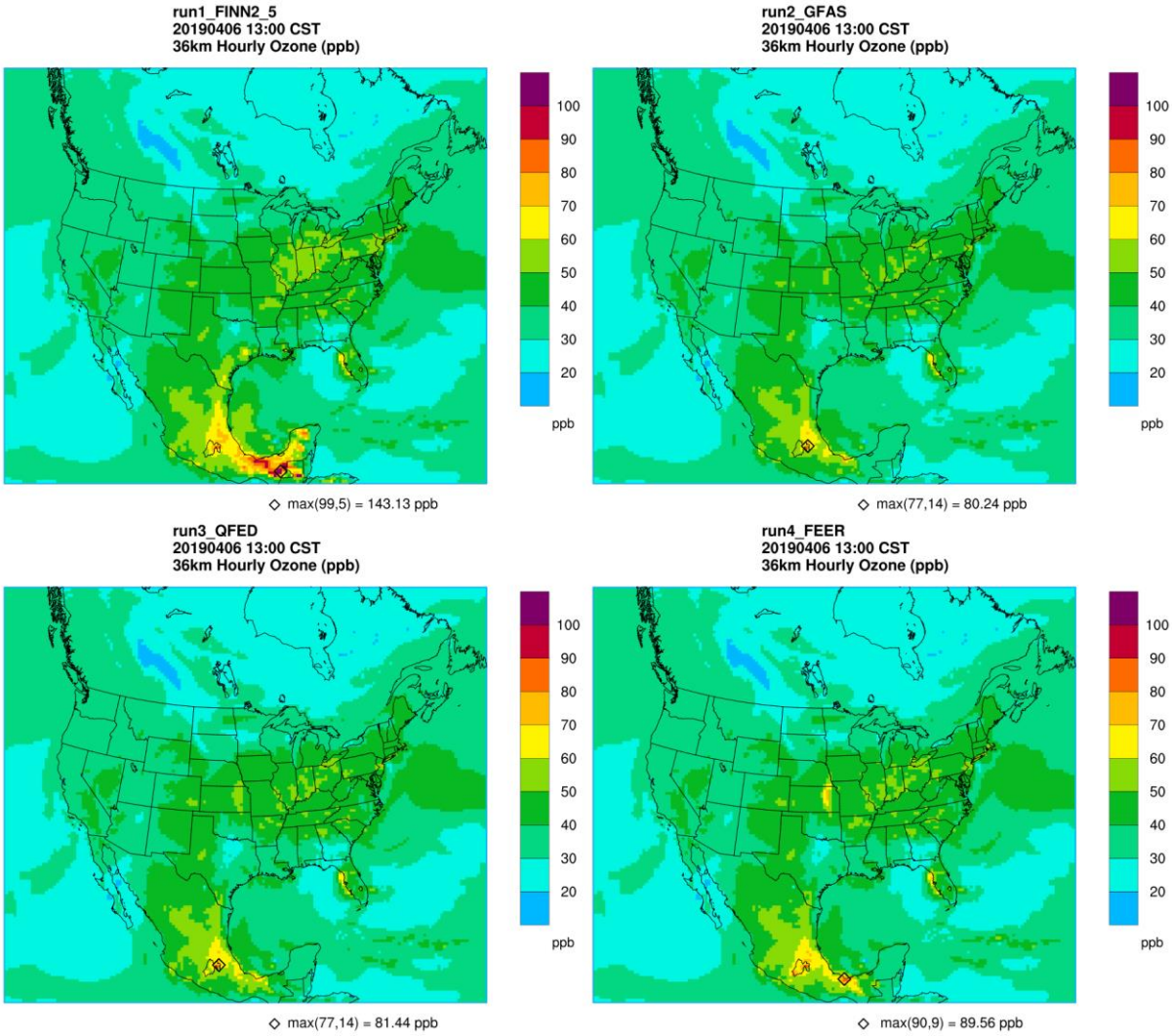

Figure 3-7. CAMx 36 km ozone concentrations for FINN2.5 (top left), GFAS1.2 (top right), QFED2.5 (bottom left) and FEER1.0 (bottom right) on April 6, 2019 at 1 PM CST.

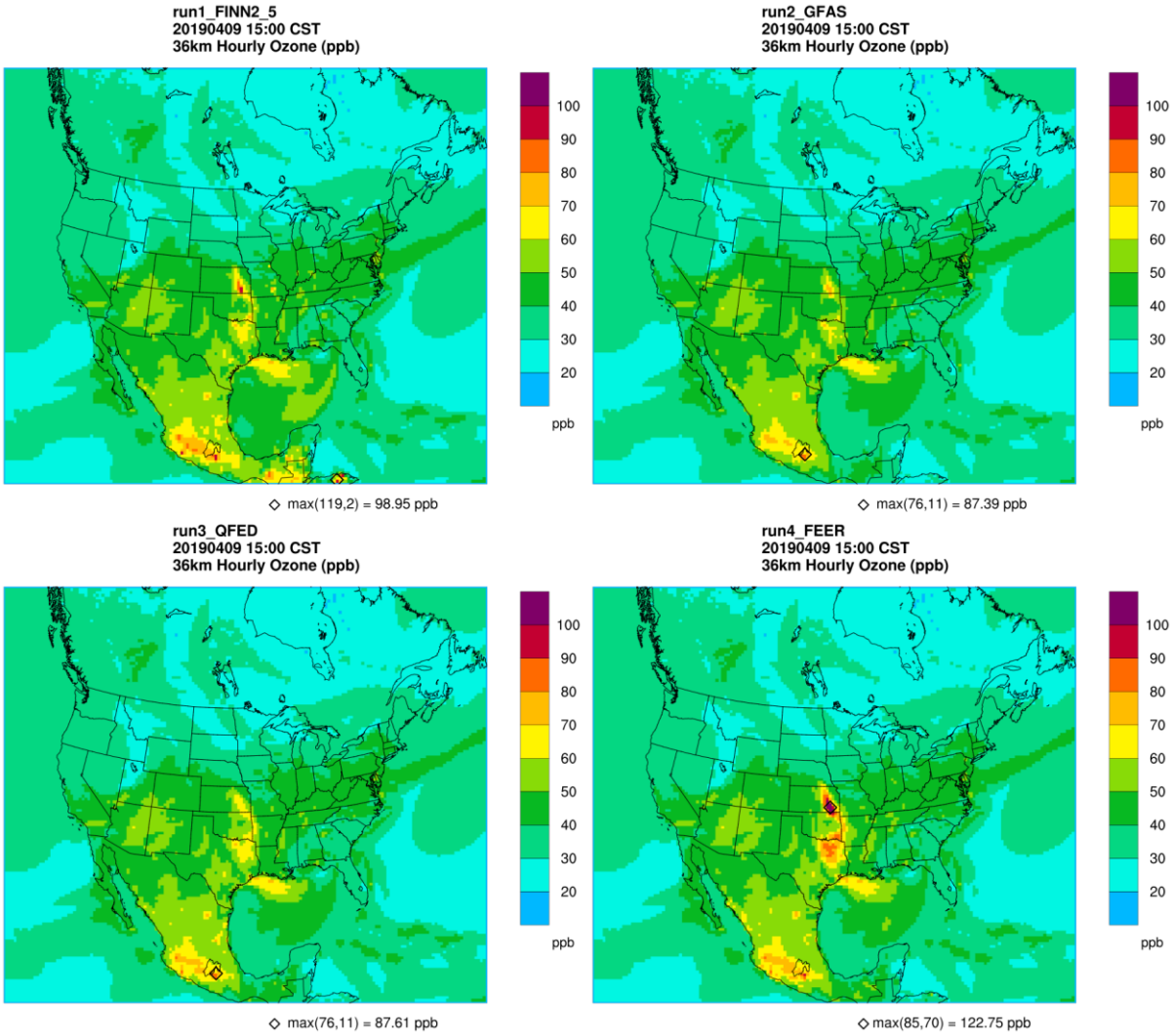

Figure 3-8. CAMx 36 km ozone concentrations for FINN2.5 (top left), GFAS1.2 (top right), QFED2.5 (bottom left) and FEER1.0 (bottom right) on April 9, 2019 at 3 PM CST.

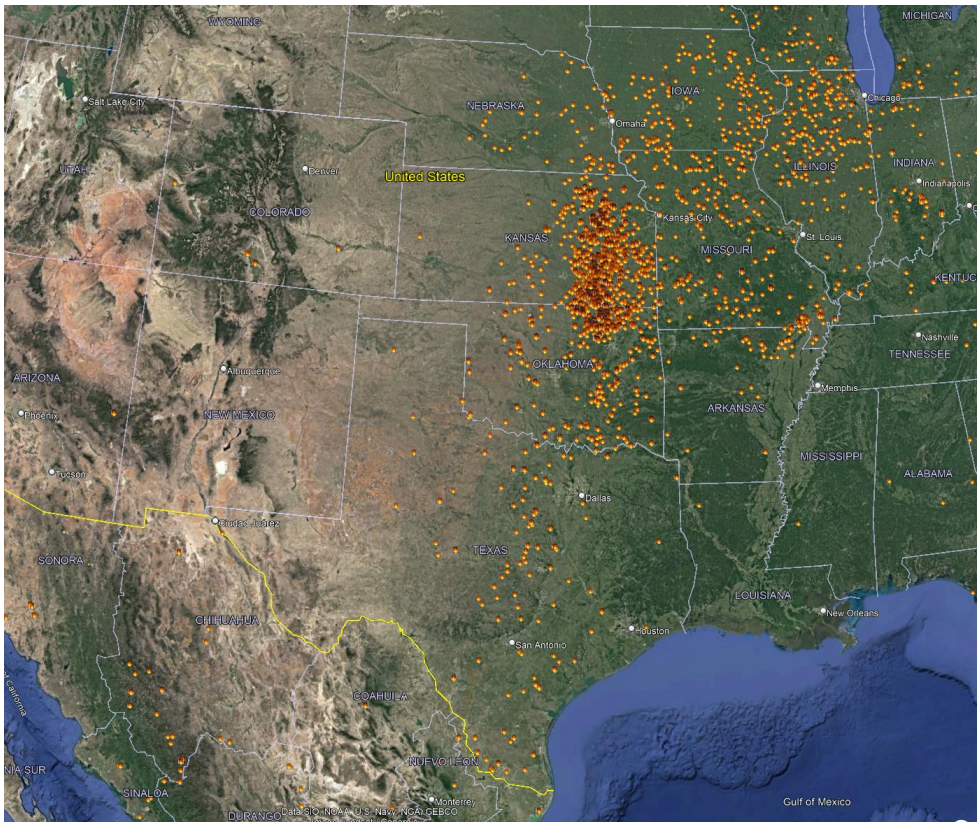

Figure 3-9. NOAA HMS detected fires for April 9, 2019.

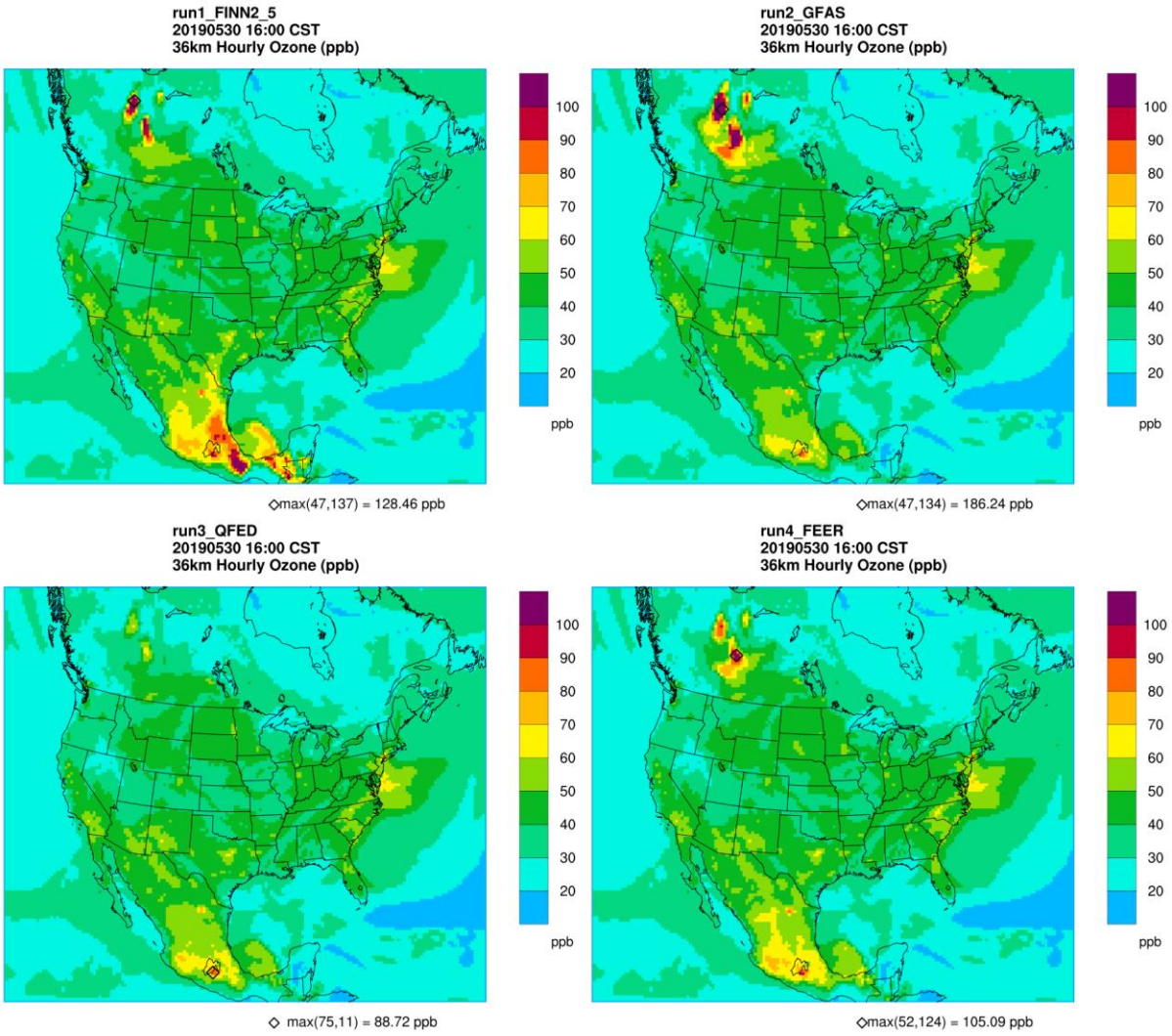

Figure 3-10. CAMx 36 km ozone concentrations for FINN2.5 (top left), GFAS1.2 (top right), QFED2.5 (bottom left) and FEER1.0 (bottom right) on May 30, 2019 at 4 PM CST.

3.2.2 Phase 2 Comparison

For phase 2, we conducted sensitivity runs designed to examine impacts of all four combinations of temporal and vertical emission allocation schemes (one of these four sensitivity tests, run2, was run in phase 1). Table 3-13 shows the region-wide statistics for each sensitivity run for the period of April 9 – May 31, 2019. Performance statistics are nearly identical across the four sensitivity tests for all regions. Figure 3-11 shows hourly ozone (top panel), ozone bias (2nd panel from top), $PM_{2.5}$ (3rd panel from top) and $PM_{2.5}$ bias (bottom panel) time series at San Antonio Northwest C23 during April 2019 for the four CAMx sensitivity tests evaluated in phase 2. Differences between the runs are extremely minor for both ozone and $PM_{2.5}$ concentrations. Conceptually, these results make sense given the long-range transport and vertical mixing of smoke from Mexico and Central America into Texas, which mitigates effects from the different temporal and vertical allocation schemes at the fire sources. We cannot make a recommendation about selection of processor configuration options based on results from this modeling episode.

Table 3-13. MDA8 ozone statistics in the Dallas-Fort Worth TCEQ Region during April 6 – May 31 period for each FEI sensitivity test based on the GFAS1.2 FEI.

FEI Temporal Option	RAVE	RAVE	DEFAULT	DEFAULT
FEI Vertical Option	**SOFIEV**	**PBL500**	**PBL500**	**SOFIEV**
Number of Observations	1066	1066	1066	1066
Mean Concentration – Observations (ppb)	44.2	44.2	44.2	44.2
Mean Concentration – Model (ppb)	41.9	41.9	42.0	42.0
R^2	0.462	0.462	0.462	0.462
Mean Bias (ppb)	-2.3	-2.3	**-2.2**	**-2.2**
Mean Error (ppb)	6.7	6.7	**6.6**	6.7
Normalized Mean Bias (%)	-5.2	-5.1	**-4.9**	-5.0
Normalized Mean Error (%)	15.2	15.1	**15.0**	15.1
Mean Fractional Bias (%)	-3.8	-3.7	**-3.5**	-3.6
Mean Fractional Error (%)	16.2	16.1	**16.0**	16.1

Table 3-14. MDA8 ozone statistics in the San Antonio TCEQ Region during April 6 – May 31 period for each FEI sensitivity test based on the GFAS1.2 FEI.

FEI Temporal Option	RAVE	RAVE	DEFAULT	DEFAULT
FEI Vertical Option	**SOFIEV**	**PBL500**	**PBL500**	**SOFIEV**
Number of Observations	658	658	658	658
Mean Concentration – Observations (ppb)	38.9	38.9	38.9	38.9
Mean Concentration – Model (ppb)	41.9	41.9	42.1	42.0
R^2	0.410	0.410	0.410	0.410
Mean Bias (ppb)	**3.0**	**3.0**	3.2	3.1
Mean Error (ppb)	**7.0**	**7.0**	7.1	7.1
Normalized Mean Bias (%)	**7.8**	**7.8**	8.2	8.1
Normalized Mean Error (%)	**18.1**	**18.1**	18.2	18.2
Mean Fractional Bias (%)	**9.9**	10.0	10.3	10.2
Mean Fractional Error (%)	**18.9**	**18.9**	19.0	19.0

Table 3-15. MDA8 ozone statistics in the Houston TCEQ Region during April 6 – May 31 period for each FEI sensitivity test based on the GFAS1.2 FEI.

FEI Temporal Option	RAVE	RAVE	DEFAULT	DEFAULT
FEI Vertical Option	**SOFIEV**	**PBL500**	**PBL500**	**SOFIEV**
Number of Observations	1943	1943	1943	1943
Mean Concentration – Observations (ppb)	40.6	40.6	40.6	40.6
Mean Concentration – Model (ppb)	41.7	41.7	41.8	41.8
R^2	0.490	0.490	0.490	0.490
Mean Bias (ppb)	**1.1**	**1.1**	1.2	1.2
Mean Error (ppb)	7.7	**7.6**	7.7	7.7
Normalized Mean Bias (%)	**2.6**	**2.6**	2.9	2.8
Normalized Mean Error (%)	**18.8**	**18.8**	18.9	18.9
Mean Fractional Bias (%)	**6.3**	**6.3**	6.6	6.5
Mean Fractional Error (%)	**20.2**	**20.2**	**20.2**	20.3

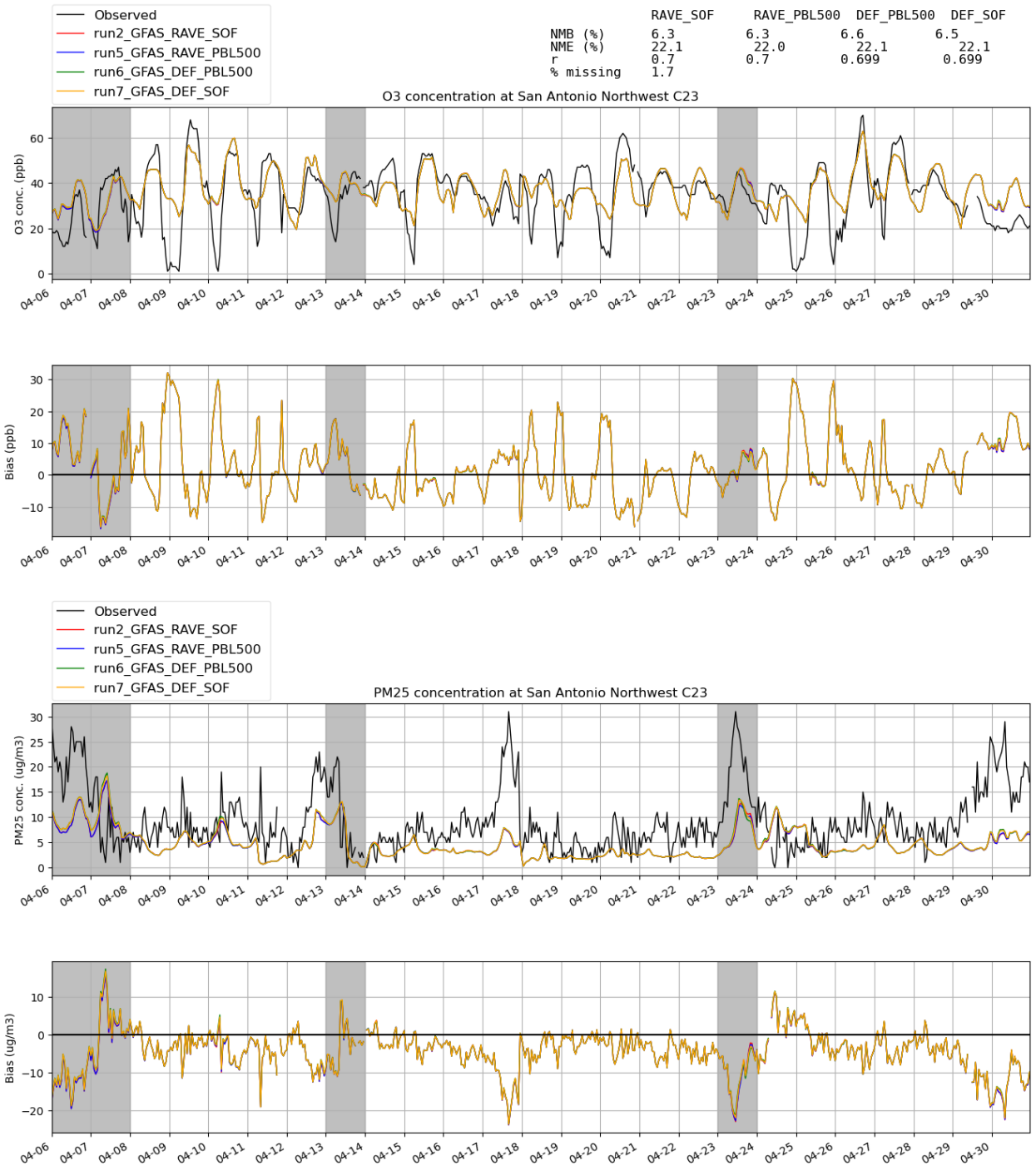

Figure 3-11. Hourly ozone (top panel), ozone bias (2nd panel from top), $PM_{2.5}$ (3rd panel from top) and $PM_{2.5}$ bias (bottom panel) time series at San Antonio Northwest C23 for April 2019. Grey shaded regions represent days when TCEQ's modeling exhibited poor ozone performance.

4.0 CONSENSUS FEI RECOMMENDATIONS

4.1 Consensus Methods

Many different ensemble methodologies have been applied for air quality and climate modeling applications (Galmarini et al., 2013; Kioutsioukis et al., 2016; Di et al., 2019; Delle Monache et al., 2020; Charn et al., 2022) to develop consensus model simulations. These methods vary in complexity, but typically involve weighting predictions from the ensemble model members in a manner that minimizes error relative to observations. Each of these studies applied ensemble methods to build a consensus simulation that outperformed any single simulation's performance. Clearly, developing a similar method to construct a consensus FEI that results in superior model performance relative to any single FEI would be ideal. However, our literature review found no such methods exist for developing a consensus of emission inventory products, including fire emission inventories. In fact, M. Sofiev (personal communication), developer of the fire plume rise parameterization evaluated in this project, does not believe ensemble methods are applicable to FEIs.

As we detail below, developing a consensus FEI presents several challenges for which there are no clear solutions.

4.2 Challenges with Development of a Consensus FEI

Developing a consensus FEI presents the following challenges:

- Ensemble methods developed for air quality or climate modeling do not lend a clear and direct translation toward the characterization of emission inventories. Primarily, these methods rely on comparison to observed conditions to minimize error. There are simply no comparable routine observations that measure a multitude of fire emissions intensity, diurnal variability, vertical distribution, or speciation. All of these characteristics must be estimated or parameterized from limited information.
- FEI emissions are too diverse; they differ among pollutant, region, and time period. Table 4-1 shows $PM_{2.5}$ and NOx emission summaries for Texas, Contiguous U.S., Mexico, and Central America for April 1 – May 31, 2019. Table 4-3 shows the same emission summaries for VOC and CO. Emissions vary by orders of magnitude among the four FEIs presented. Any method used to construct a consensus FEI would have to account for these differences in a reasonable and objective way.
- FINN2.5 (as well as earlier versions) exhibits a known problem in classifying gas flares as fires (Ramboll, 2022b; Johnson et al. 2019). Our analysis has shown that GFAS1.2 and QFED2.5 do not show these same detection errors (we have not yet examined FEER emissions for this same issue). All satellite products used to derive fire emissions are prone to false alarms, which can include reflected solar radiation from solar panels, hot and bright surfaces and cloud glint[13]. A consensus strategy would ideally exclude these false alarms, but no such strategy exists.

[13] https://vlab.noaa.gov/web/towr-s/viirs-active-fires

- The FEIs used in this study are continually updated. The processing of raw satellite measurements, along with other inputs such as landcover information and emission factors change over time. Therefore, any consensus FEI developed would have to be reevaluated frequently.
- Any consensus strategy would be based on a limited comparison. The modeling period used in this study is for a two-month period in a single year using a single air quality model. Model performance evaluation is limited to ozone and $PM_{2.5}$ at monitoring sites in Texas. Depending on how a "consensus" is defined and developed, the resulting consensus FEI may not lead to the best air quality model performance, especially if outlier FEIs such as FINN carry sufficient weight. Conclusions about model performance, and therefore choices about how to construct a consensus FEI, may change for a different year, season, pollutant, or region.

Table 4-1. $PM_{2.5}$ emissions summaries for FINN2.5, GFAS1.2, QFED2.5, and FEER1.0 for April 1 – May 31, 2019.

Region	FINN2.5	GFAS1.2	QFED2.5	FEER1.0
Texas	4,516	2,724	13,933	7,270
Contiguous U.S.	169,625	67,396	368,972	179,157
Mexico	1,818,459	340,120	1,563,697	881,844
Central America	424,538	74,048	177,758	137,466

Table 4-2. NOx emissions summaries for FINN2.5, GFAS1.2, QFED2.5, and FEER1.0 for April 1 – May 31, 2019.

Region	FINN2.5	GFAS1.2	QFED2.5	FEER1.0
Texas	2,250	824	4,211	3,598
Contiguous U.S.	52,654	17,182	81,051	76,946
Mexico	636,730	75,396	233,510	373,756
Central America	160,778	13,616	24,055	48,592

Table 4-3. VOC emissions summaries for FINN2.5, GFAS1.2, QFED2.5, and FEER1.0 for April 1 – May 31, 2019.

Region	FINN2.5	GFAS1.2	QFED2.5	FEER1.0
Texas	20,595	3,963	3,801	82,572
Contiguous U.S.	805,903	95,140	83,616	2,182,318
Mexico	10,656,403	575,285	346,877	11,593,469
Central America	2,695,650	146,271	52,859	2,026,089

Table 4-4. CO emissions summaries for FINN2.5, GFAS1.2, QFED2.5, and FEER1.0 for April 1 – May 31, 2019.

Region	FINN2.5	GFAS1.2	QFED2.5	FEER1.0
Texas	39,706	32,705	67,365	88,308
Contiguous U.S.	1,470,334	719,470	1,409,053	2,102,134
Mexico	16,592,452	3,746,423	5,353,945	10,665,411
Central America	3,984,321	824,422	779,715	1,648,940

5.0 CONCLUSIONS AND RECOMMENDATIONS

In the first phase of this project, Ramboll updated the Python FEI processor to include: 1) the FEER1.0 FEI; 2) a new temporal allocation option based on the RAVE landcover-specific diurnal profiles; and 3) a new vertical plume rise scheme.

As requested by TCEQ, we applied TCEQ's modeling platform for April-May 2019, replacing only the fire emissions generated by the recently updated Python FEI processor. TCEQ's modeling using CAMx showed large positive ozone biases related to FINN fire emissions throughout April and May of 2019 when transport of smoke from biomass burning in Mexico and Central America was frequent.

Our testing confirmed that FINN2.5 resulted in similarly large positive ozone biases. However, the three Fire Radiative Power (FRP)-based FEIs (GFAS1.2, QFED2.5, FEER1.0) all showed substantially smaller ozone biases and overall better statistical agreement with observations. We identified GFAS1.2 as the best representation of fires due to overall ozone model performance and its reporting of useful parameters such as FRP and vertical plume information. We then conducted additional testing using fire emission inputs based on all four combinations of vertical and temporal allocation schemes applied to the GFAS1.2 FEI. Ozone and $PM_{2.5}$ concentrations were nearly identical across the four tests given long range transport that moderates effects from plume rise and temporal treatments. Therefore, we cannot make recommendations from these tests regarding optimal processor configuration options.

Finally, Ramboll evaluated potential methods, benefits and challenges involved in developing a consensus FEI. After a literature review and consideration of the limitations of the FEIs as well as our limited modeling application, we cannot recommend a particular strategy for developing a consensus FEI. We therefore recommend GFAS1.2 as an alternative to a consensus approach. This recommendation is based on the two-month period evaluated in this study and could change pending additional modeling for different years, seasons, or regions.

Ramboll recommends three activities to improve the FEI processor and support TCEQ's needs:

- Code modifications to process RAVE1.0, a newly released FEI, that could provide better fire emissions estimates for those fires that contribute wildfire smoke into Texas.
- Investigate performance of vertical plume rise (the Sofiev scheme) and temporal allocation schemes for Texas fires near monitor locations.
- Conduct CAMx simulations for additional seasons and years using all available FEIs, including RAVE if available, and evaluate ozone and $PM_{2.5}$ model performance against observations.

6.0 VIRTUAL WORKSHOPS ON BEST PRACTICES FOR MODELING

Ramboll prepared and participated in three TCEQ-led virtual training workshops for TCEQ staff on general best practices in modeling. Each session was led by a 3- or 4-person panel comprised of representatives from Ramboll, TCEQ, and EPA, with specific examples from past projects. The format of each involved a free-form interactive discussion and Q&A with attendees. The group allowed for questions related to each topic to be submitted to the panelists and distributed to attendees before each session so examples/answers could be prepared beforehand.

Topics covered in the workshops included meteorological modeling and photochemical modeling addressing ozone and particulate matter (PM). The workshops included discussions on issues related to evaluating model performance, model configuration inputs and options, common pitfalls, approaches that have worked best over combined decades of TCEQ, EPA, and consultant experience, new issues concerning PM emissions preparation and modeling, and associated sensitivity responses. The details of each training workshop, including length, content, panelists, and presentation material, were discussed and agreed upon with TCEQ managers in preparation for each session. All three workshop were hosted and recorded by TCEQ using the Microsoft Teams virtual meeting platform. All presentation material is archived by the TCEQ for future use. Logistical and topical details for each workshop are provided below.

Workshop 1: Meteorological Modeling

This session included an introduction and free-form discussion on best practices when utilizing the WRF model for air quality applications. Participants were given the opportunity to ask questions and discuss various topics with the panelists.

- Date/Time: Thursday, April 20, 1-4 PM CDT
- Moderator: Bryce Kuchan, TCEQ
- Panel Participants: Jeremiah Johnson (Ramboll), Robert Gilliam (EPA), Khalid Al-Wali (TCEQ), Doug Boyer (TCEQ)
- Planned topics (not all topics were covered in the time given):
  - Understanding Model Capabilities and Limitations:
    - Input data sources, resolution, and relative importance (terrain, SST, analyses for IC/BC and FDDA)
    - Relative importance of configuration options, where/when to apply each (physics, FDDA methods, advantages/disadvantages, data requirements), runtime impacts, known sensitivities
    - Nesting options (1- vs. 2-way feedback) and recommendations for best practices
    - Selecting specific output variable fields needed for photochemical modeling (rainfall accumulation, sub-grid convection, etc.)
  - Model Evaluation, Pitfalls and Best Practices:

- Beyond the cookie-cutter stats, dig into additional details, how to investigate specific issues/problems, things to consider
- Qualitative precipitation analyses, boundary layer evolution, best sources of observed data (routine and special study)
- How model configuration or sources of input data can influence the performance evaluation
- Running WRF in parallel using 5.5-day increments vs. singularly running whole period

Workshop 2: Photochemical Modeling for Ozone

This session included an introduction and free-form discussion on best practices when utilizing CAMx and other AQ models for ozone air quality applications. Participants were given the opportunity to ask questions and discuss various topics with the panelists.

- Date/Time: Monday, May 8, 1-4 PM CDT
- Moderator: Bryce Kuchan, TCEQ
- Panel Participants: Chris Emery (Ramboll), Heather Simon (EPA), Weining Zhao (TCEQ), Beata Czader (TCEQ)
- Planned topics (not all topics were covered in the time given):
  - Understanding Model Capabilities and Limitations
    - Where are photochemical grid models useful vs. not useful (and even misleading)
    - Resolution limits at both small and large scales, vertical layer collapsing, mitigating differences in "off-line" (meteorologically decoupled) model applications
    - Understanding Plume-in-Grid, advantages and drawbacks – is it still relevant?
    - Input data sources and relative importance (met, emissions, landcover, photolysis)
    - Understanding vertical diffusion rates and model sensitivity
    - Relative importance of configuration options, where/when to apply each (chemistry options, horizontal and vertical transport schemes, PiG, deposition and surface model), runtime impacts, known sensitivities
    - Parallelization options and planned updates
  - Model Evaluation, Pitfalls and Best Practices
    - Beyond the cookie-cutter stats, dig into additional details, how to investigate specific issues/problems, things to consider
    - The pragmatic use of statistical performance benchmarks – what do they really mean?
    - How model configuration and optional treatments can influence MPE
    - Chemical evaluations, indicator ratios, VOC comparisons, chemical process analysis
    - The current state-of-science for assessing performance against satellite products

Workshop 3: Photochemical Modeling for PM

This session included an introduction and free-form discussion on modeling particulate matter. Participants were given the opportunity to ask questions and discuss various topics with the panelists.

- Date/Time: Thursday, June 1, 1-4 PM CDT
- Moderator: Bryce Kuchan, TCEQ
- Panel Participants: Chris Emery (Ramboll), Colleen Baublitz (EPA), Bob Gifford (TCEQ)
- Planned topics (not all topics were covered in the time given):
  - New NAAQS, future PM nonattainment areas, and air quality issues for Texas (beyond regional fire smoke influences)
  - PM species and state of current science represented in modeling
  - Ammonia emissions and deposition as key influences on secondary inorganic PM
  - Characterizing emissions and chemistry of organic PM and precursors
  - Other natural PM emissions: sea salt, windblown dust
  - Uncertainties in speciating gas precursors from fire emissions
  - Additional modeling/MPE considerations beyond those for ozone

7.0 REFERENCES

Andela, N., Kaiser, J.W., Heil, A., Van Leeuwen, T.T., van der Werf, G.R., Wooster, M.J., Remy, S. and Schultz, M.G., 2013. Assessment the Global Fire Assimilation System (GFASv1).

Briggs, G. 1975. Plume rise predictions. In 'Lectures on air pollution and environmental impact analyses'. (Ed. Haugen D) pp. 59–111 (American Meteorological Society: Boston, MA, USA).

Charn, A.B., O'Brien, T.A., Risser, M.D., Longmate, J.M. and Feldman, D.R., 2022. Sign of Observed California Temperature Trends Depends on Data Set Homogenization: Implications for Weighting and Downscaling. Geophysical Research Letters, 49(15), p.e2022GL099186.

Darmenov, A. and da Silva, A. 2015. The quick fire emissions dataset (QFED) – Documentation of versions 2.1, 2.2 and 2.4. NASA//TM-2015-104606, Vol. 38, NASA Global Modeling and Assimilation Office, 183 pp., https://gmao.gsfc.nasa.gov/pubs/docs/Darmenov796.pdf

Delle Monache, L., Alessandrini, S., Djalalova, I., Wilczak, J., Knievel, J.C. and Kumar, R., 2020. Improving air quality predictions over the United States with an analog ensemble. Weather and Forecasting, 35(5), pp.2145-2162.

Di, Q., Amini, H., Shi, L., Kloog, I., Silvern, R., Kelly, J., Sabath, M.B., Choirat, C., Koutrakis, P., Lyapustin, A. and Wang, Y., 2019. An ensemble-based model of $PM_{2.5}$ concentration across the contiguous United States with high spatiotemporal resolution. Environment international, 130, p.104909.

Galmarini, S., Kioutsioukis, I. and Solazzo, E., 2013. E pluribus unum*: ensemble air quality predictions. Atmospheric Chemistry and Physics, 13(14), pp.7153-7182.

Ichoku, C. and Ellison, L. 2014. Global top-down smoke-aerosol emissions estimation using satellite fire radiative power measurements, Atmos. Chem. Phys., 14, 6643–6667, https://doi.org/10.5194/acp-14-6643-2014.

Johnson, J., E. Tai, P. Karamchandani, G. Wilson, G. Yarwood. 2013. "TCEQ Ozone Forecasting System." Prepared for Texas Commission on Environmental Quality, Austin, TX. November.

Johnson, J., G. Wilson, D.J. Rasmussen, G. Yarwood. 2015. "Daily Near Real-Time Ozone Modeling for Texas." Prepared for Texas Commission on Environmental Quality, Austin, TX. January.

Johnson, J., G. Wilson, D.J. Rasmussen, G. Yarwood. 2016. "Daily Near Real-Time Ozone Modeling for Texas." Prepared for Texas Commission on Environmental Quality, Austin, TX. January.

Johnson, J., G. Wilson, J. Bandoro, K. Richman, L. Huang, R. Beardsley and G. Yarwood. 2018. Near-Real Time Exceptional Event Modeling. Prepared for Mark Estes, TCEQ. August.

Johnson, J., G. Wilson, M. Jimenez, T. Shah, R. Beardsley, K. Richman and G. Yarwood. 2017. Fire Impact Modeling with CAMx. Prepared for Mark Estes, TCEQ. July.

Johnson, J., G. Wilson, S. Kemball-Cook, K. Tanner, Y. Shi, J. Guo, R. Beardsley and G. Yarwood. 2019. Near Real-Time Exceptional Event Modeling. Prepared for Mark Estes, TCEQ. August.

Kioutsioukis, I., Im, U., Solazzo, E., Bianconi, R., Badia, A., Balzarini, A., Baró, R., Bellasio, R., Brunner, D., Chemel, C. and Curci, G., 2016. Insights into the deterministic skill of air quality ensembles from the analysis of AQMEII data. Atmospheric Chemistry and Physics, 16(24), pp.15629-15652.

Li, F., X. Zhang, S. Kondragunta, X. Lu, I. Csiszar, C. C. Schmidt. 2022. Hourly biomass burning emissions product from blended geostationary and polar-orbiting satellites for air quality forecasting applications. Remote Sensing of Environment. https://doi.org/10.1016/j.rse.2022.113237.

McDonald-Buller, E., Y. Kimura, C. Wiedinmyer, C. Emery, Z. Liu and G. Yarwood. 2015. Targeted Improvements in the Fire INventory from NCAR (FINN) Model for Texas Air Quality Planning. Prepared for David Sullivan, Texas Air Quality Research Program and The University of Texas at Austin. August.

Ramboll, 2020. Near Real-Time Exceptional Event Modeling. Prepared for Erik Gribbin, TCEQ. November.

Ramboll, 2022a. Develop Carbon Bond Version 7 Revision 1 (CB7r1) for CAMx Ozone Modeling, Report for TCEQ Work Order 582-22-31131-025, June 2012.

Ramboll. 2022b. Develop Tools to Process and Evaluate Options for Improved Fire Emission Inventories. Ramboll US Consulting, Inc., Novato CA. Prepared for the Texas Commission on Environmental Quality. June 24.

Ramboll. 2022c. User's Guide – Comprehensive Air Quality Model with Extensions Version 7.20. Available at www.camx.com. April 2022.

Randles, C. A., da Silva, A. M., Buchard, V., Colarco, P. R., Darmenov, A., Govindaraju, R., Smirnov, A., Holben, B., Ferrare, R., Hair, J., Dhinozuka, Y., and Flynn, C. J. 2017. The MERRA-2 aerosol reanalysis, 1980 onward. Part I: system description and data assimilation evaluation, J. Climate, 30, 6823–6850, https://doi.org/10.1175/JCLI-D-16-0609.1.

Rienecker, M. M., Suarez, M. J., Gelaro, R., Todling, R., Bacmeister, J., Liu, E., Bosilovich, M. G., Schubert, S. D., Takacs, L., Kim, G.-K., Bloom, S., Chen, J., Collins, D., Conaty, A., da Silva, A., Gu, W., Joiner, J., Koster, R. D., Lucchesi, R., Molod, A., Owens, T., Pawson, S., Pegion, P., Redder, C. R., Reichle, R., Robertson, F. R., Ruddick, A. G., Sienkiewicz, M., and Woollen, J. 2011. MERRA – NASA's Modern-Era Retrospective Analysis for Research and Applications, J. Climate, 24, 3624–3648.

Rémy, S., Veira, A., Paugam, R., Sofiev, M., Kaiser, J. W., Marenco, F., Burton, S. P., Benedetti, A., Engelen, R. J., Ferrare, R., and Hair, J. W. 2017. Two global data sets of daily fire emission injection heights since 2003, Atmos. Chem. Phys., 17, 2921–2942, https://doi.org/10.5194/acp-17-2921-2017.

Skamarock, W. C., Klemp, J. B., Dudhia, J., Gill, D. O., Liu, Z., Berner, J., Wang, W., Powers, J. G., Duda, M. G., Barker, D., Huang, X.Y. 2021. A Description of the Advanced Research WRF Model Version 4.3 (No. NCAR/TN-556+STR). Doi:10.5065/1dfh-6p97

Sofiev, M., Ermakova, T., & Vankevich, R. 2012. Evaluation of the smoke-injection height from wild-land fires using remote-sensing data. Atmospheric Chemistry and Physics, 12(4), 1995–2006. https://doi.org/10.5194/acp-12-1995-2012

van Leeuwen, T.T., van der Werf, G.R., Hoffmann, A.A., Detmers, R.G., Rücker, G., French, N.H., Archibald, S., Carvalho Jr, J.A., Cook, G.D., de Groot, W.J. and Hély, C., 2014. Biomass burning fuel consumption rates: a field measurement database. Biogeosciences, 11(24), pp.7305-7329.

Wilkins, J. L., Pouliot, G., Pierce, T., Soja, A., Choi, H., Gargulinski, E., Gilliam, R., Vukovich, J., Landis, M. S. 2022. An evaluation of empirical and statistically based smoke plume injection height parametrisations used within air quality models. International Journal of Wildland Fire 31, 193-211. https://doi.org/10.1071/WF2014.

Appendix A Additional Ozone and $PM_{2.5}$ Time Series

This Appendix includes ozone and $PM_{2.5}$ time series for Calaveras Lake C59 and ozone time series for Camp Bullis C58, Grapevine Fairway C70 and Dallas Redbird Airport C402.

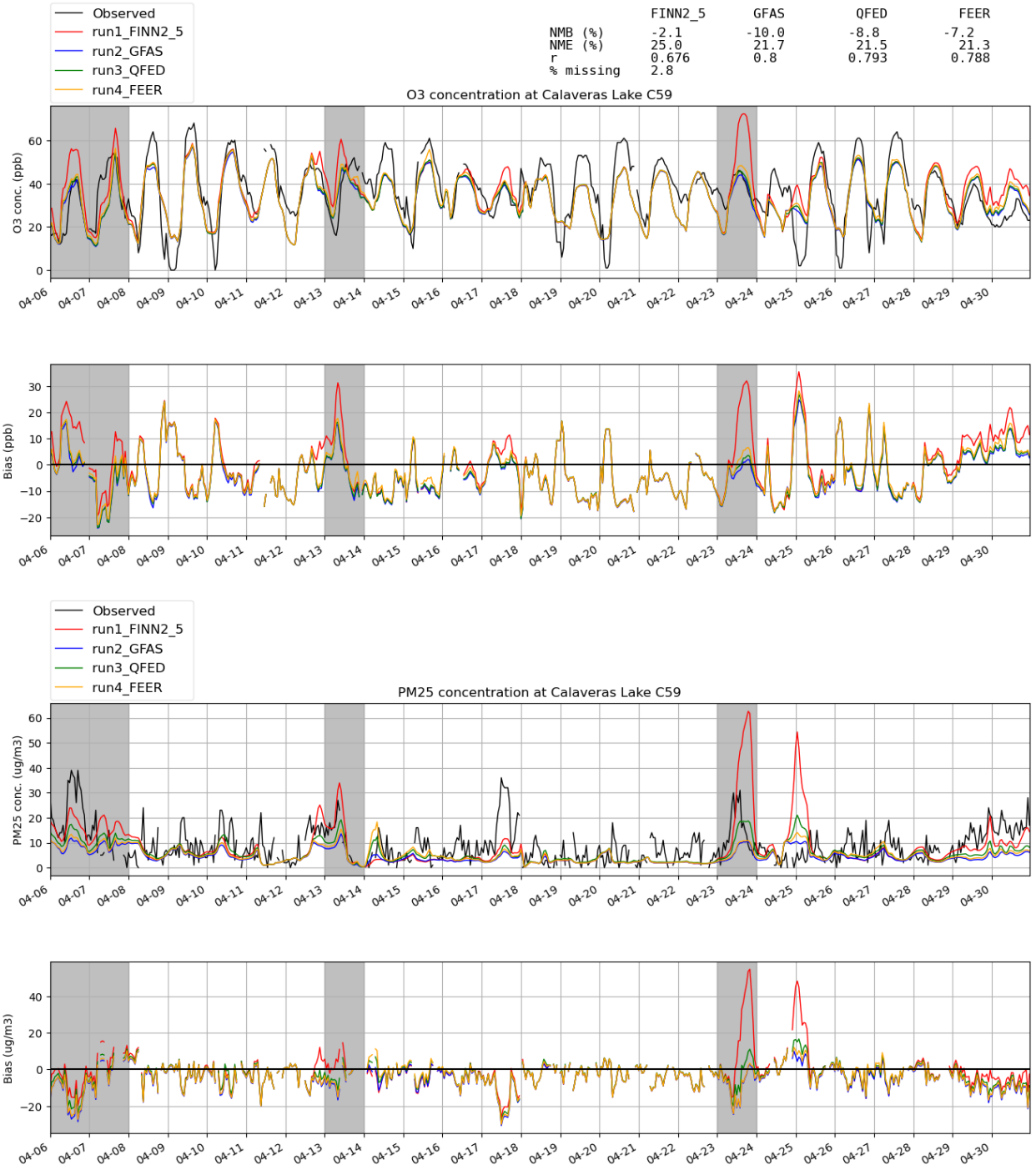

Figure A-1. Hourly ozone (top panel), ozone bias (2nd panel from top), $PM_{2.5}$ (3rd panel from top) and $PM_{2.5}$ bias (bottom panel) time series at Calaveras Lake C59 for April 2019. Grey shaded regions represent days when TCEQ's modeling exhibited poor ozone performance.

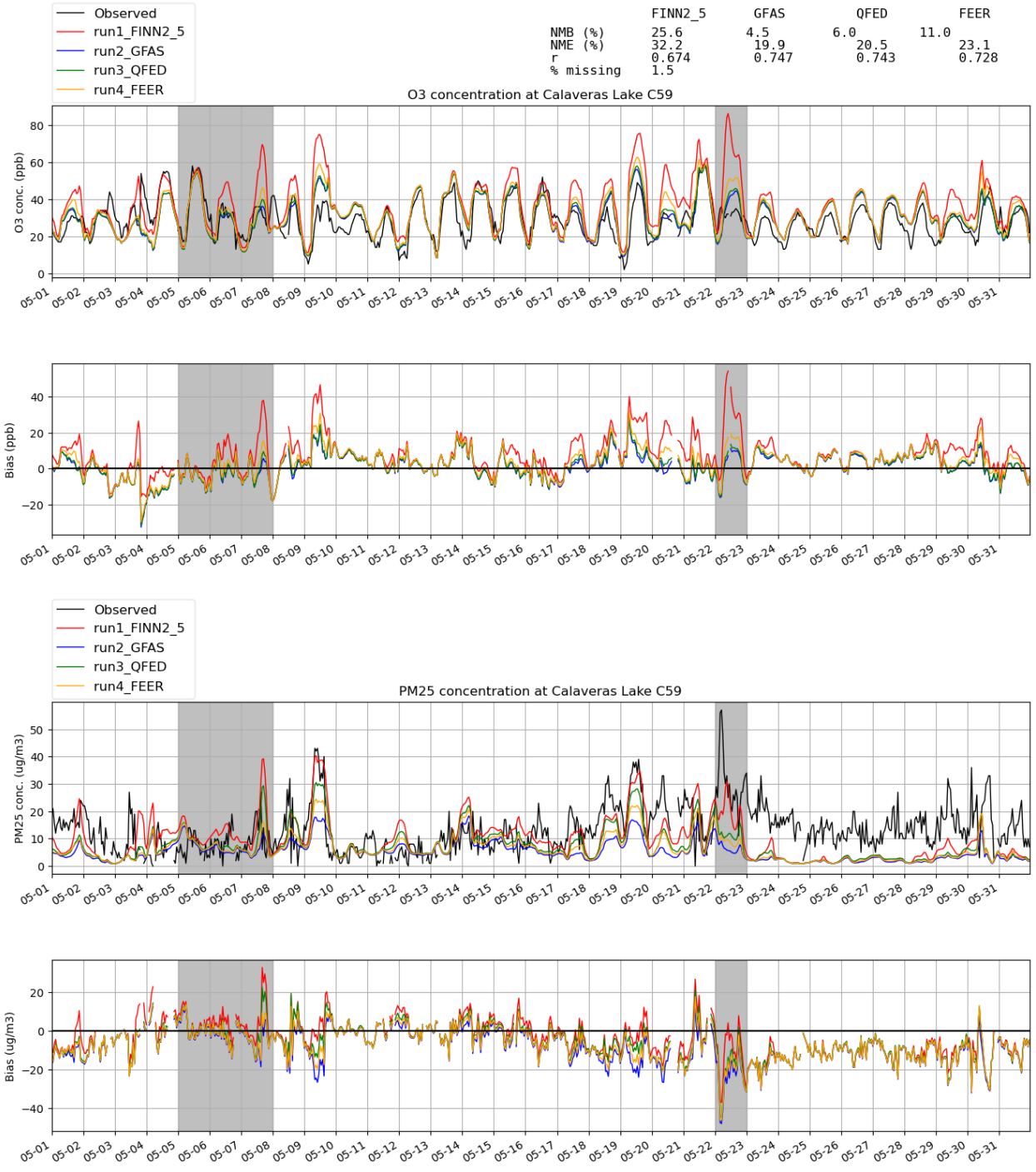

Figure A-2. Hourly ozone (top panel), ozone bias (2nd panel from top), $PM_{2.5}$ (3rd panel from top) and $PM_{2.5}$ bias (bottom panel) time series at Calaveras Lake C59 for May 2019. Grey shaded regions represent days when TCEQ's modeling exhibited poor ozone performance.

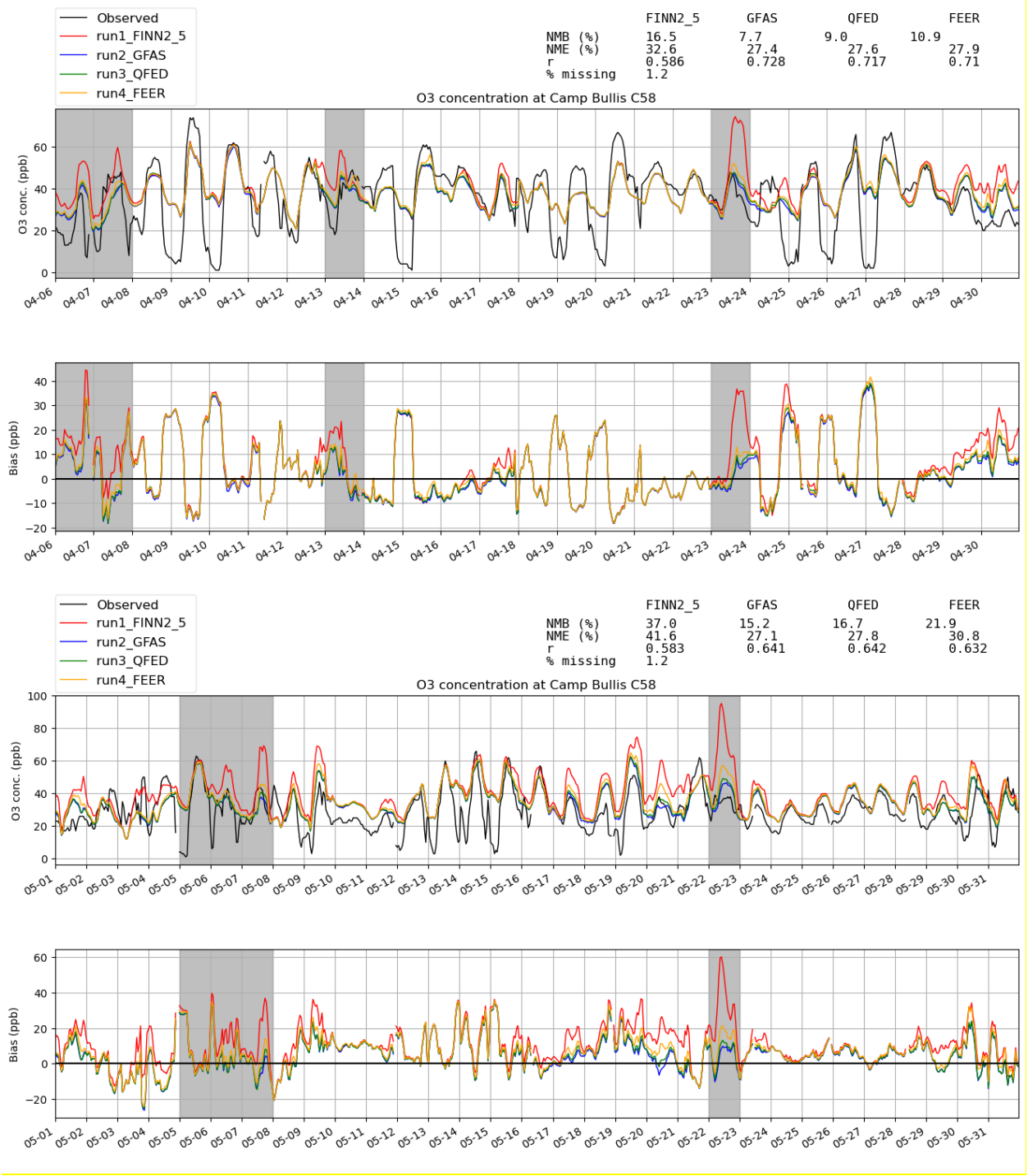

Figure A-3. April 2019 hourly ozone (top panel), ozone bias (2nd panel from top) and May 2019 ozone (3rd panel from top) and ozone bias (bottom panel) time series at Camp Bullis C58. Grey shaded regions represent days when TCEQ's modeling exhibited poor ozone performance.

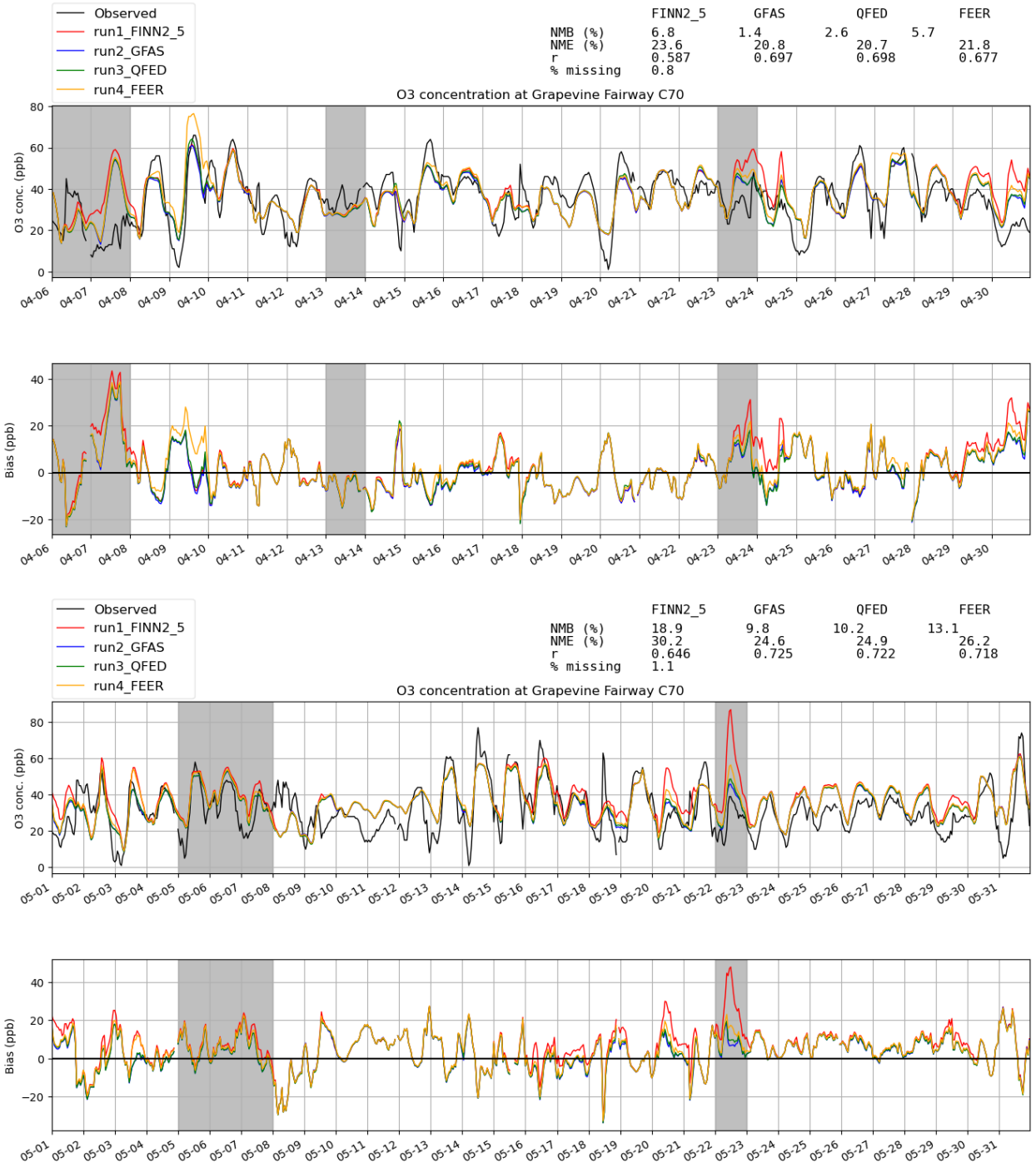

Figure A-4. April 2019 hourly ozone (top panel), ozone bias (2nd panel from top) and May 2019 ozone (3rd panel from top) and ozone bias (bottom panel) time series at Grapevine Fairway C70. Grey shaded regions represent days when TCEQ's modeling exhibited poor ozone performance.

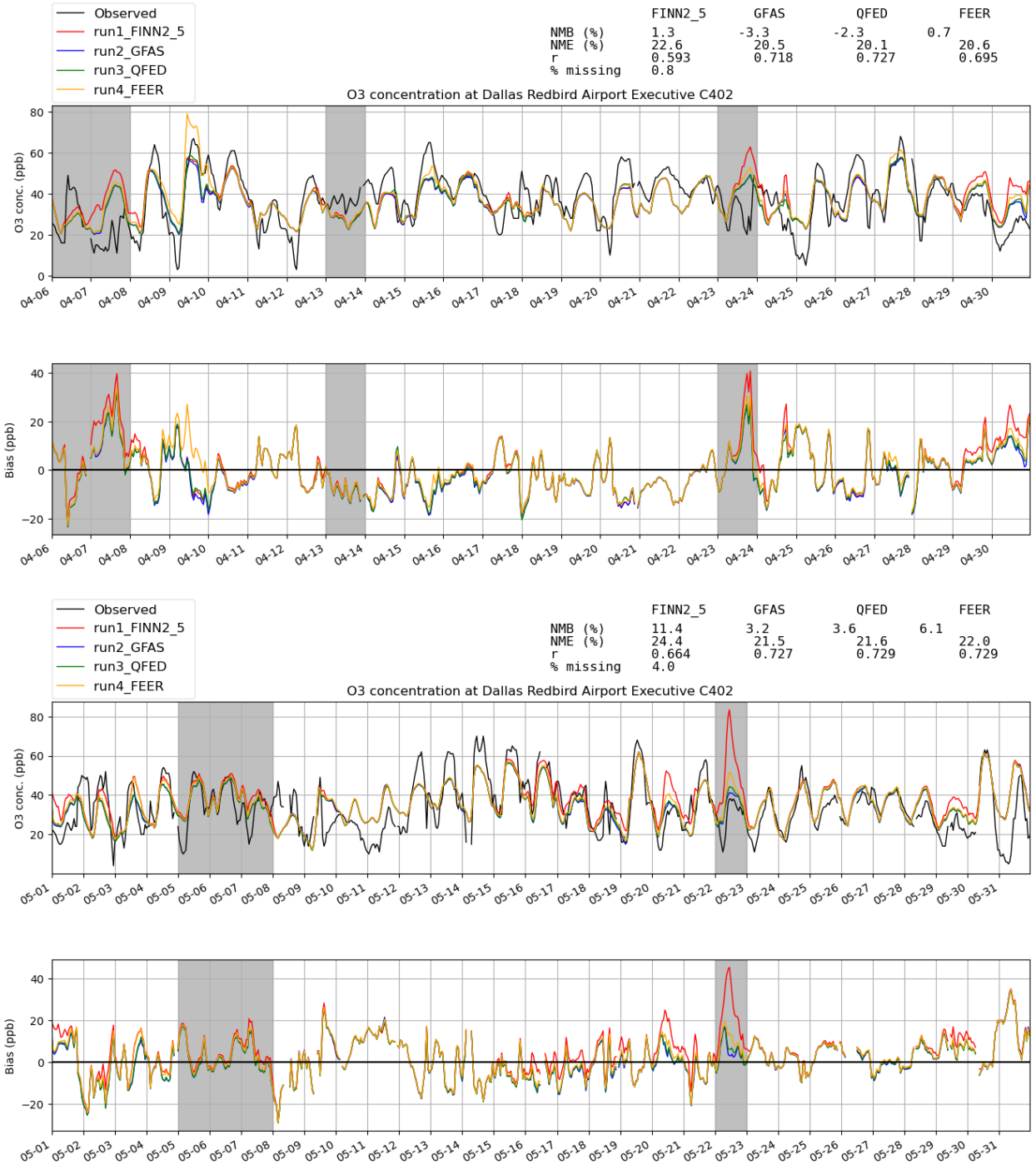

Figure A-5. April 2019 hourly ozone (top panel), ozone bias (2nd panel from top) and May 2019 ozone (3rd panel from top) and ozone bias (bottom panel) time series at Dallas Redbird Airport Executive C402. Grey shaded regions represent days when TCEQ's modeling exhibited poor ozone performance.